BEYOND CONFLICT: SUBSPACE-ALIGNMENT AS THE MISSING PIECE OF MODEL MERGING

Anonymous authors
Paper under double-blind review

ABSTRACT

Model merging integrates task knowledge by combining task vectors (differences between pre-trained and fine-tuned weights) across models for both vision and large language models (LLMs). Existing methods improve merging performance solely by mitigating conflicts between task vectors. However, we find that conflict alone is not the full story: when conflict-oriented remedies are applied, severe interference still persists. This observation motivates a novel perspective: analysing the interference from the standpoint of alignment. Experiments reveal that task vectors exhibit high alignment in subspaces with large singular values. After merging, these aligned subspaces gather more singular values and produce activations with higher magnitude compared to others. The resulting spectral imbalance substantially degrades model performance. Inspired by this, in contrast to previous methods that focus solely on conflicts, we propose the Subspace-Alignment Aware Merging (AlignMerge), which quantifies alignment by projecting task vectors onto the shared singular subspaces of the merged task vector and attenuates overly aligned components. AlignMerge is training-free and requires no auxiliary data. Across vision and language benchmarks, it achieves state-of-the-art performance and narrows the gap to traditional multi-task learning to 3.6%.

1 INTRODUCTION

Model merging fuses trained models directly in weight space into a single model (Ruan et al., 2025). Rather than retraining models from scratch or relying on traditional model ensembling, model merging enables the direct manipulation and fusion of model weights to combine capabilities (Shah et al., 2025; Ortiz-Jimenez et al., 2023), forget detrimental knowledge (Ilharco et al., 2022; Ni et al., 2024), or mitigate catastrophic forgetting between tasks (Chitale et al., 2023; Marczak et al., 2025b). Model merging not only dramatically accelerates the development of large-scale models, such as large language models (LLMs) (Goddard et al., 2024; Wan et al., 2024), but also unlocks unprecedented flexibility in leveraging collective model intelligence (Huang et al., 2024; Oh et al., 2024). Current research primarily focuses on merging models that were fine-tuned on different tasks but share the same pre-trained backbone, yielding a single model with stronger multi-task capability. Furthermore, many of these works are based on the analysis and utilisation of task vectors (Ilharco et al., 2022), which are defined as the difference between pre-trained and fine-tuned weights.

Currently, most task-vector based methods attribute interference in model merging to a variety of conflict (*e.g.*, weight or singular conflict (Yadav et al., 2023; Gargiulo et al., 2025)). *Yet task vectors are nearly orthogonal (Ortiz-Jimenez et al., 2023), so large conflicts should be rare, yet interference persists, even when conflict-oriented remedies are applied.* Therefore, we propose a question: Is there any other factors beyond conflict, contribute to the interference? To uncover the underlying factors, we approach the problem from the opposite direction and analyse the **Alignment**. For clarity, we henceforth reshape each task vector into its matrix form. As illustrated in Fig. 1(b), an SVD of these task vectors reveals pronounced alignment in the top singular subspaces across both vision and language backbones (details in the Appendix). We term this phenomenon subspace-alignment. When task vectors are summed, components within the aligned subspaces add coherently, resulting in a substantial increase in the singular values of these subspaces relative to others (Fig. 1(c)). This, in turn, significantly amplifies activations of aligned subspaces during inference and degrades accuracy. The resulting spectral imbalance accumulation cautions against global scaling across subspaces and motivates a targeted remedy: attenuate overly aligned components in different subspaces.

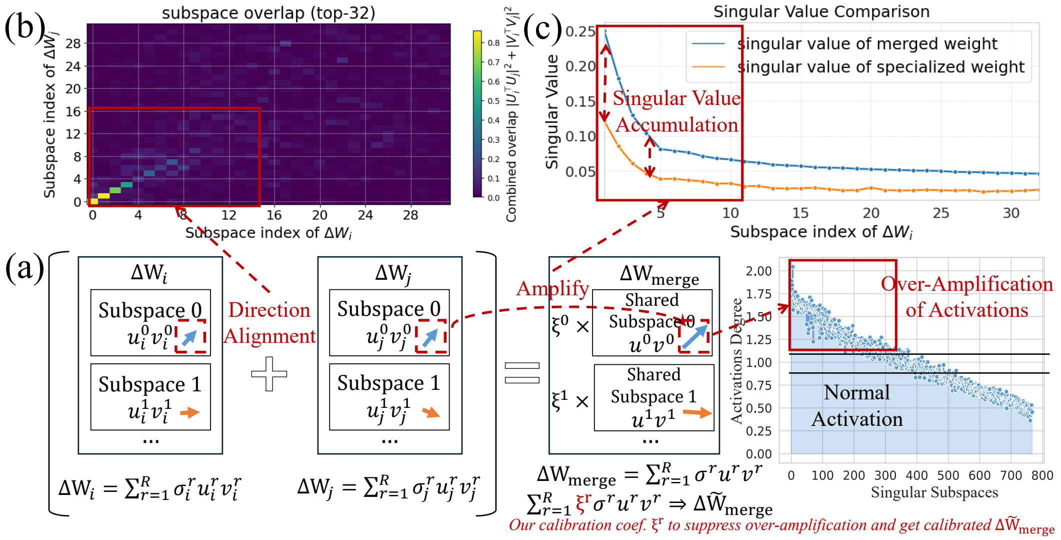
(b)
subspace overlap (top-32)
Subspace index of ΔW_j
Subspace index of ΔW_i
Combined overlap $|U_i^\top U_j|^2 + |V_i^\top V_j|^2$
(c)
Singular Value Comparison
singular value of merged weight
singular value of specialized weight
Singular Value
Singular Value Accumulation
Subspace index of ΔW_i
(a)
ΔW_i
Subspace 0
$u_i^0 v_i^0$
Subspace 1
$u_i^1 v_i^1$
Direction Alignment
ΔW_j
Subspace 0
$u_j^0 v_j^0$
Subspace 1
$u_j^1 v_j^1$
Amplify
ΔW_{merge}
Shared Subspace 0
$\xi^0 \times$ $u^0 v^0$
Shared Subspace 1
$\xi^1 \times$ $u^1 v^1$
$\Delta W_i = \sum_{r=1}^{R} \sigma_i^r u_i^r v_i^r$
$\Delta W_j = \sum_{r=1}^{R} \sigma_j^r u_j^r v_j^r$
$\Delta W_{\text{merge}} = \sum_{r=1}^{R} \sigma^r u^r v^r$
$\sum_{r=1}^{R} \xi^r \sigma^r u^r v^r \Rightarrow \Delta \widetilde{W}_{\text{merge}}$
Activations Degree
Over-Amplification of Activations
Normal Activation
Singular Subspaces
Our calibration coef. ξ^r to suppress over-amplification and get calibrated $\Delta \widetilde{W}_{\text{merge}}$

Figure 1: (a) Overview of the alignment across singular subspaces. Applying subspace calibration coefficients ξ^r yields the corrected $\Delta\widetilde{\mathbf{W}}_{\text{merge}}$. (b) Similarity between two task vectors, measured by $S = \|U_A^\top U_B\|_F^2 + \|V_A^\top V_B\|_F^2$, where U and V are left/right singular vectors of the task vector. (c) Projecting the summed task vector onto each specialized task vector's subspace shows that stronger alignment yields greater singular-value accumulation within that subspace.

Specifically, in this paper, we focus on the shared singular subspaces obtained by applying SVD to the summed task vector $\Delta\mathbf{W}_{\text{merge}}$. We project any pair of task vector, $\Delta\mathbf{W}_i$ and $\Delta\mathbf{W}_j$, onto this common basis and compute a Subspace Cross-Influence $\xi_{i,j}^r$. Visualizing $\xi_{i,j}^r$ (Fig. 2) shows that subspaces with larger singular values tend to exhibit stronger alignment.

Motivated by these observations, we design two distinct *Subspace-alignment Aware Merging (AlignMerge)* strategies at pre/post-merging stages. At the **post-merging stage**, building on Marczak et al. (2025a) who observe gains from averaging singular values, *AlignMerge through Balancing (AlignMerge-B)* rescales each singular subspace using a calibration coefficient ξ^r computed from pairwise Subspace Cross-Influence $\{\xi_{i,j}^r\}$. This subspace normalization suppresses over-amplification in highly aligned directions and improves overall accuracy.

At the **pre-merging stage**, by explicitly enforcing task vector orthogonality among all subspaces via whitening, *AlignMerge through orthogonalisation (AlignMerge-O)* can effectively eliminate the alignment of task vectos in different subspaces. Overall, AlignMerge-O substantially mitigates the activation over-amplification induced by subspace-alignment; however, by operating on weights in isolation, it limits the exploitation of shared structure and cross-task transfer. Extensive experiments validate the critical role of these effects and show that AlignMerge consistently achieves SOTA performance on diverse benchmarks. In summary, our research makes three key contributions:

1) We find that conflict explains only the tip of the interference iceberg; a substantial, overlooked portion arises from the alignment of task vectors within singular subspaces.

2) We propose two *Subspace-alignment Aware Merging (AlignMerge)* strategies at different stages, to effectively mitigate the over-amplification of activations caused by highly aligned subspaces.

3) Both theoretical analysis and experiments demonstrate the effectiveness of AlignMerge, reducing the performance gap to conventional MTL to just 3.6%, while also enabling targeted enhancement for specific tasks (*i.e.*, Preference Optimisation).

In this paper, Section 2 reviews related work. Section 3 formalizes subspace-alignment and analyses its impact on model merging. Building on these insights, Section 4 introduces two methods that mitigate alignment-induced interference.

2 RELATED WORK

Dynamic Model Merging. Unlike model ensembling, which combines the outputs or predictions of multiple independent models to improve generalisation (Dong et al., 2020), model merging operates directly at the weight level. In its common training-free (Zhang et al., 2025; Li et al., 2025; Yuan et al., 2025) form, it integrates the knowledge encoded in the parameters of several trained models into a single unified model (Yang et al., 2024a). This technology addresses challenges such as catastrophic forgetting (Chitale et al., 2023; Zhu et al., 2024; Marczak et al., 2025b), domain shift (Izmailov et al., 2019; Wortsman et al., 2022), and the efficient construction of LLMs (Dekoninck et al., 2024; Aiello et al., 2023). To reduce conflicts among models, a line of work studies dynamic merging, where the behaviour of the merged model depends on the input. For example, DaWin (Oh et al., 2024) performs input-conditioned interpolation, EMR-Merging (Huang et al., 2024) and TALL-Mask (Wang et al., 2024) learn task-specific masks, and Twin-Merging (Lu et al., 2024) introduces task experts in the spirit of mixture-of-experts. These approaches often achieve strong performance, but they rely on task or routing information at inference, which limits practicality.

Static Model Merging. Early research primarily focused on weight averaging or traditional interpolation strategies (Wortsman et al., 2022; Ilharco et al., 2022; Matena & Raffel, 2022; Jin et al., 2023), enabling rapid assembly of models with diverse task expertise but often suffering from suboptimal performance due to unresolved conflicts or redundancies among weights. Subsequent research has sought to mitigate inter-model conflicts under either data-dependent or data-free regimes. Data-dependent methods rely on auxiliary data such as validation sets or unlabeled test inputs. For example, PCB-Merging (Du et al., 2024) uses a validation set, NPS-Pruning (Du et al., 2025) employs a calibration set, and AdaMerging (Yang et al., 2024c) and Trust Region Arithmetic (Sun et al., 2025) perform test-time adaptation. Such dependencies reduce practical applicability in settings without accessible auxiliary data. Data-free methods can be grouped into weight-space and singular-vector perspectives. Weight-space methods (Yu et al., 2024; Yadav et al., 2023; He et al., 2024) localise and prune conflicting parameters to reduce incompatibility, while SVD-based approaches (Gargiulo et al., 2025; Stoica et al., 2024; Marczak et al., 2025a) focus on spectral alignment to reconcile conflicts at the subspace level. However, existing research focuses exclusively on various forms of conflict, overlooking the fact that subspace-alignment can also introduce inter-model interference and ultimately degrade performance.

3 WHAT CAUSE INTER-MODEL INTERFERENCE

Building on the preliminaries (Sec. 3.1), we formalize what subspace-alignment is and its measurement (Sec. 3.2), and then analyse how Subspace-Alignment cause interference (Sec. 3.3).

3.1 PRELIMINARY

Given a set of K model parameter set $\{\mathbf{W}_i\}_{i=1}^{K}$, which fine-tuned on pre-trained parameter $\mathbf{W}_{\text{pre}}$. Model merging aims to construct a merged model $\mathbf{W}_{\text{merge}}$ that integrally inherits task-specific knowledge from all $\{\mathbf{W}_i\}$. Traditionally, a simple weight averaging is adopted: $\mathbf{W}_{\text{merge}} = \frac{1}{K}\sum_{i=1}^{K}\mathbf{W}_i$. Building on this, Task Arithmetic (TA) (Ilharco et al., 2022) introduces the concept of task vector $\Delta\mathbf{W}_i = \mathbf{W}_i - \mathbf{W}_{\text{pre}}$, and then applies a function $\mathcal{F}$ to merge task vectors, yielding $\Delta\mathbf{W}_{\text{merge}} = \mathcal{F}(\Delta\mathbf{W}_1, \Delta\mathbf{W}_2, \ldots, \Delta\mathbf{W}_K)$. Finally, with an additional hyperparameter λ, model merging can be achieved in the following paradigm:

$$\mathbf{W}_{\text{merge}} = \mathbf{W}_{\text{pre}} + \lambda\Delta\mathbf{W}_{\text{merge}}. \tag{1}$$

However, this strategy fails to capture the inherent relationship between weights. Recent developments represent weight matrices in spectral form, typically via singular value decomposition (SVD) (Gargiulo et al., 2025):

$$\Delta\mathbf{W}_i = \mathbf{U}_i\mathbf{\Sigma}_i\mathbf{V}_i^{\top} = \sum_{r=1}^{R}\sigma_i^r\boldsymbol{u}_i^r(\boldsymbol{v}_i^r)^{\top} = \sum_{r=1}^{R}\sigma_i^r\mathbf{M}_i^r, \tag{2}$$

where $\mathbf{U}_i$ and $\mathbf{V}_i$ denote the left and right singular vectors, and $\mathbf{\Sigma}_i$ is a diagonal matrix of singular values. This decomposition can also be viewed as a weighted sum of R outer products of singular vectors, which are the spans of the rank-one matrix $\mathbf{M}_i^r$ we called **singular vector subspace**.

For subsequent analysis, for 2 **rank-one matrices** $\mathbf{A}$ and $\mathbf{B}$, we define the Frobenius inner product-based projection coefficient $\mathbf{A}$ onto another matrix $\mathbf{B}$ as $\mathrm{Proj}_{\mathbf{B}}(\mathbf{A})$, which measures the alignment between two matrices and equals the projection between singular vectors (Details in Appendix B.1):

$$\mathrm{Proj}_{\mathbf{B}}(\mathbf{A}) = \frac{\langle \mathbf{A}, \mathbf{B} \rangle_F}{\langle \mathbf{B}, \mathbf{B} \rangle_F} = \frac{\mathrm{tr}(\mathbf{A}^\top \mathbf{B})}{||\mathbf{B}||_F^2}. \tag{3}$$

3.2 Subspace-Alignment Causes Interference

Model merging aims to combine the capabilities of specialized models into a single model. In practice, inter-model interference can cause these capabilities to cancel, so simple weight averaging often underperforms. Prior works largely attribute such interference to conflicts among task vectors (Yadav et al., 2023; Yu et al., 2024), yet severe degradation still remains after conflict-oriented remedies. This observation raises the question: Is there any other factors beyond conflict, contribute to the interference? We therefore examine the interference from the opposite direction, alignment.

As shown in Fig. 1(b), performing an SVD of each task vector in matrix form and comparing their left and right singular subspaces reveals a clear pattern: although task vectors are approximately orthogonal (Ilharco et al., 2022), their SVD-defined subspaces exhibit strong directional alignment. Further investigation of this alignment property demonstrates that stronger alignment in a subspace between the specialised models leads to larger singular-value growth of their merged model in that subspace, which inflates activations at inference. However, The alignment is highly non-uniform, high in the top singular subspaces and much weaker in lower ones (Fig. 1(b), Fig. 6). As a result,the accumulation of singular values across subspaces in the merged model varies significantly (Fig. 1(c)), leading to dominance of highly aligned subspaces and suppression of those with low alignment during inference. These observations motivate estimating alignment per subspace and applying targeted corrections to highly aligned components to prevent over-accumulation.

Based on this, model merging can be reformulated from the perspective of subspace. Specifically, let $\Delta\mathbf{W}_{\text{merge}}$ denote the merged model, obtained by applying an arbitrary merging function to K specialized models $\{\Delta\mathbf{W}_1, \dots, \Delta\mathbf{W}_K\}$. Through singular value decomposition (SVD), $\Delta\mathbf{W}_{\text{merge}}$ can then be represented as a sum over multiple shared subspaces $\mathbf{M}_{\text{merge}}^r = \boldsymbol{u}_{\text{merge}}^r(\boldsymbol{v}_{\text{merge}}^r)^\top$, then we consider each subspace $\mathbf{M}_{\text{merge}}^r$ as the projection of each specialized task vector $\{\Delta\mathbf{W}_k\}_{k=1}^K$ through projection matrices $\mathbf{P}_{\text{col}}^r = \boldsymbol{u}_{\text{merge}}^r(\boldsymbol{u}_{\text{merge}}^r)^\top$ and $\mathbf{P}_{\text{row}}^r = \boldsymbol{v}_{\text{merge}}^r(\boldsymbol{v}_{\text{merge}}^r)^\top$.

$$\Delta\mathbf{W}_{\text{merge}} = \mathbf{U}_{\text{merge}}\mathbf{\Sigma}_{\text{merge}}\mathbf{V}_{\text{merge}} = \sum_{r=1}^{R} \sigma_{\text{merge}}^r \mathbf{M}_{\text{merge}}^r = \sum_{r=1}^{R} \eta^r \sum_{i=1}^{K} \mathbf{P}_{\text{col}}^r \Delta\mathbf{W}_i \mathbf{P}_{\text{row}}^r, \tag{4}$$

where $\eta^r = \sigma_{\text{merge}}^r / \left((\boldsymbol{u}_{\text{merge}}^r)^\top \sum_{i=1}^K \Delta\mathbf{W}_i \boldsymbol{v}_{\text{merge}}^r \right)$ serves as a scaling factor. To assess the relationship between $\Delta\mathbf{W}_j$ and $\Delta\mathbf{W}_i$ within the shared subspace $\mathbf{M}_{\text{merge}}^r$, and how this alignment amplify activation magnitudes at inference, we establish the following proposition, whereby the Subspace Cross-Influence $\xi_{i,j}^r$ of how task j influence on task i in shared subspace r is derived.

Proposition 1 (Subspace Cross-Influence) *Let $\Delta\mathbf{W}_i$ and $\Delta\mathbf{W}_j$ be 2 task vectors finetuned from different tasks, the extent that task j influence on task i within shared subspace r can be calculated as Subspace Cross-Influence $\xi_{i,j}^r$ (The definition of $\mathbf{W}_{\text{res}}^r$ and other details defer in Appendix B.2):*

$$\xi_{i,j}^r = \mathrm{Proj}_{\mathbf{P}_{\text{col}}^r\, \mathbf{\Delta W}_i}\left(\mathbf{P}_{\text{col}}^r\, \mathbf{\Delta W}_j\right) + \mathrm{Proj}_{\mathbf{W}_i^r\, \mathbf{P}_{\text{row}}^r}\left(\mathbf{W}_{\text{res}}^r\, \mathbf{P}_{\text{row}}^r\right). \tag{5}$$

$$\mathbf{P}_{col}^r \Delta\mathbf{W}_j \mathbf{P}_{row}^r \approx \xi_{i,j}^r \mathbf{P}_{col}^r \Delta\mathbf{W}_i \mathbf{P}_{row}^r \tag{6}$$

For Subspace Cross-Influence $\xi_{i,j}^r$, a positive value indicates alignment between tasks i and j in subspace r. The overlapping component of $\Delta\mathbf{W}_j$ then adds coherently to $\Delta\mathbf{W}_i$ at inference (*i.e.*,

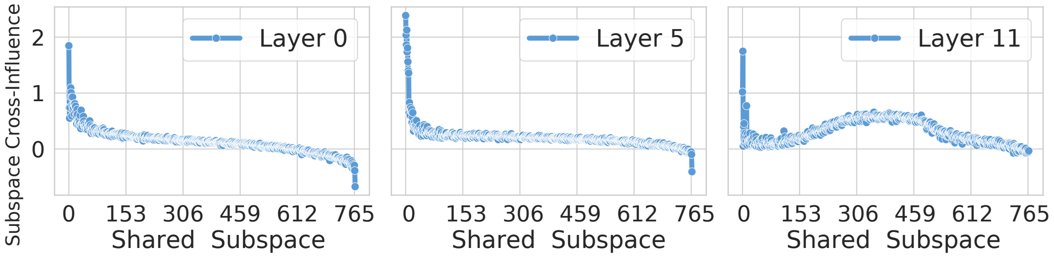

Figure 2: Visualisation of Subspace Cross-Influence of layer 'mlp.c_proj.weight', illustrating the impact of MNIST on Cars. Notably, subspace with lower index correspond to larger singular values.

"double counting"), amplifying activations in that subspace. We visualize the $\xi^r_{i,j}$ across different subspaces in Fig. 2. The pattern mirrors Fig. 6: positive alignment is concentrated in shared subspaces with large singular values and decays as the singular values decrease.

3.3 How Subspace-Alignment Cause Interference

After computing the Subspace Cross-Influence coefficients $\xi^r_{i,j}$, the whole influence on target task i in subspace r is $\sum_{j\neq i} \xi^r_{i,j}$. By combining with Eq.(4), the merged task vector in the shared subspace r can be represented as the projection of the task vector only corresponding to task i:

$$\sigma^r_{\text{merge}}\,\mathbf{M}^r_{\text{merge}} \approx \eta^r \left(\sum_{j=1,\, j\neq i}^{K} \xi^r_{i,j} + 1 \right) \mathbf{P}^r_{\text{col}}\,\boldsymbol{\Delta}\mathbf{W}_i\,\mathbf{P}^r_{\text{row}} \tag{7}$$

Proposition 2 (Optimal subspace coefficient) *Let* $\mathbf{S} = \sum_{r=1}^{R} \xi^r\, \mathbf{P}^r_{\text{col}} \Delta \mathbf{W}^r_i \mathbf{P}^r_{\text{row}}$, *where* ξ^r *denotes the full coefficient in Eq. 7 before* $\mathbf{P}^r_{col}$. *Then* $\|\Delta \mathbf{W}_i - \mathbf{S}\|_F$ *is minimised if* $\xi^r = 1$ *for all* r.

Proof 2 *The above problem can be formulated as the following optimisation problem:*

$$\min_{\boldsymbol{\Sigma}} \ \|\boldsymbol{\Delta}\mathbf{W}_i - \mathbf{S}\|_F^2\,, \quad \text{s.t.} \quad \mathbf{S} = \mathbf{U}_{\text{merge}}\,\boldsymbol{\Sigma}\,\mathbf{V}_{\text{merge}}, \quad \boldsymbol{\Sigma} \text{ is diagonal.}$$

This problem admits a closed-form solution (Details in Appendix B.3), given by

$$\boldsymbol{\Sigma} = \text{diag}\left(\mathbf{U}^\top_{\text{merge}}\,\Delta\mathbf{W}_i\,\mathbf{V}_{\text{merge}}\right), \qquad \boldsymbol{\Sigma}^r = \boldsymbol{u}^\top_{\text{merge}}\,\Delta\mathbf{W}_i\,\boldsymbol{v}_{\text{merge}}.$$

When $\xi^r = 1$, *the singular value corresponding to rank* r *is exactly* $\boldsymbol{u}^\top_{\text{merge}}\,\mathbf{W}_i\,\boldsymbol{v}_{\text{merge}}$, *thereby ensuring optimal similarity. Therefore, the optimal choice is* $\xi^r = 1$ *for all* r.

By Proposition 2, as the full coefficient ξ^r approaches one, the distance $\|\Delta\mathbf{W}_{\text{merge}} - \Delta\mathbf{W}_i\|_F$ decreases. We therefore define the *Subspace-Alignment Index (SAI)* as the absolute deviation of the full coefficient from one:

$$SAI^r_i = \left| \eta^r \left(\sum_{j=1,\, j\neq i}^{K} \xi^r_{i,j} + 1 \right) - 1 \right|. \tag{8}$$

Lower SAI^r_i values indicate less interference for task i within subspace r.We visualize the signed SAI^r_i (without absolute value) for representative baselines in Fig. 3 on ViT-B/32 and Llama2-7B. Simple weight averaging (WA) reduces interference in top singular subspaces but over-suppresses bottom subspaces with weaker alignment. Task Arithmetic (TA) assigns larger scaling coefficients to task vectors, preventing over-suppression in the bottom subspaces and better balancing corrections across the spectrum, thereby reducing overall interference. TIES mitigates conflicts via weight-space pruning, likewise driving SAI^r_i closer to zero.

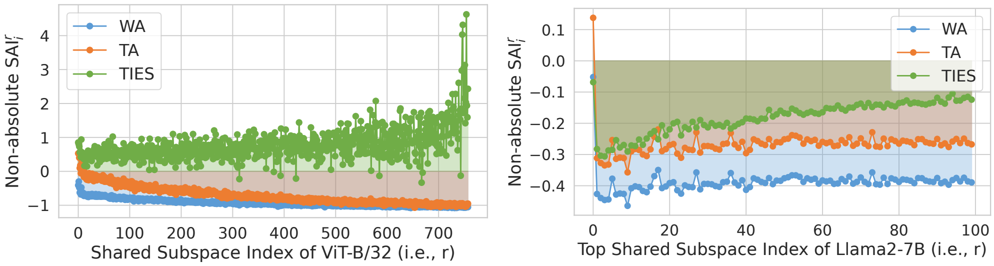

Figure 3: Visualization of non-absolute SAI_i^r across subspaces, indicating the influence of all other models on the target; values closer to 0 denote lower interference. Left: ViT-B/32. Right: Llama2.

4 Methodology

As shown above, alignment within singular subspaces can degrade the merged model's performance. We propose two complementary strategies. In post-merging stage, AlignMerge-B rescales each shared subspace using the Subspace Cross Influence (Sec. 4.1). In pre-merging stage, AlignMerge-O orthogonalizes the task vector subspaces to remove shared alignment prior to combination (Sec. 4.2).

4.1 Subspace-alignment Aware Merging Through Balancing (AlignMerge-B)

At the **post-merging stage**, the most direct way to eliminate the impact of subspace-alignment on a specific task i is to divide the merged model's singular value σ^r_{merge} in Eq. (7) by the full coefficient $\tilde{\xi}^r_i = \eta^r(\sum_{j=1,\, j\neq i}^{K} \xi^r_{i,j} + 1)$, thereby ensuring SAI^r_i equals to zero.

To control the strength of the calibration, we introduce a gating hyperparameter α. Specifically, we rescale only those subspaces with $\tilde{\xi}^r_i > \alpha$. For $\tilde{\xi}^r_i \le 0$, which indicates that $\Delta\mathbf{W}_i$ is non-contributory in that subspace, we set the corresponding component to zero. Formally,

$$\Delta\widetilde{\mathbf{W}}_{\text{merge}} = \sum_{r=1}^{R} \frac{\sigma^r_{\text{merge}}}{d(\tilde{\xi}^r_i)} \mathbf{M}^r_{\text{merge}}, \quad d(\tilde{\xi}^r_i) = \begin{cases} \tilde{\xi}^r_i, & \text{if } \tilde{\xi}^r_i \ge \alpha \\ 1, & \text{if } 0 \le \tilde{\xi}^r_i < \alpha \\ \infty. & \text{if } \tilde{\xi}^r_i \le 0 \end{cases} \tag{9}$$

When aiming to improve the performance of multiple tasks simultaneously, $\tilde{\xi}^r$ can be set as the average of $\tilde{\xi}^r_i$ across different tasks i, and substituted for $\tilde{\xi}^r_i$ in Eq. (9) accordingly.The final weights are then obtained by $\mathbf{W}_{\text{merge}} = \mathbf{W}_{\text{pre}} + \Delta\widetilde{\mathbf{W}}_{\text{merge}}$.

4.2 Subspace-alignment Aware Merging Through Orthogonalisation (AlignMerge-O)

At the **pre-merging stage**, subspace-alignment can also be eliminated by orthogonalizing singular subspaces across different specialised models. Consequently, Eq. (4) can be rewritten as

$$\sigma^r_{\text{merge}}\mathbf{M}^r_{\text{merge}} = \eta^r \mathbf{P}^r_{\text{col}} \Delta\mathbf{W}^r_{i^*} \mathbf{P}^r_{\text{row}} \text{ where } i^* = \arg\max_i \|\mathbf{P}^r_{\text{col}} \Delta\mathbf{W}^r_i \mathbf{P}^r_{\text{row}}\|_F \tag{10}$$

In this case, each singular subspace is contributed by a single model, which removes cross-model alignment and yields $\mathrm{SAI}^r_i = 0$. This also explains the effectiveness of TSV-M (Gargiulo et al., 2025). However, enforcing fully orthogonality limits the exploitation of shared structure and weakens cross-task transfer. Instead, we retain and inject a selected set of aligned subspaces into the merged model, while correcting their singular magnitudes with the scaling factor η^r.

As shown in Fig. 2, the top singular vectors of weights from different tasks generally exhibit strong alignment. To avoid information loss in these strongly aligned subspaces caused by forced orthogonalisation, we first explicitly extract their aligned subspace. Specifically, we perform SVD on each task-specific weight matrix, obtaining $\mathbf{U}_i = [\ldots, \boldsymbol{u}_i^r, \ldots, \boldsymbol{u}_i^R], \mathbf{\Sigma}_i = [\ldots, \sigma_i^r, \ldots, \sigma_i^R], \mathbf{V}_i = [\ldots, \boldsymbol{v}_i^r, \ldots, \boldsymbol{v}_i^R]$. We retain the top rank-1 singular triplets to form aligned singular vectors $\boldsymbol{u}_{\text{top}}$, $\boldsymbol{v}_{\text{top}}$ and aligned singular value σ_{top}:

$$\boldsymbol{u}_{\text{top}} = \frac{\sum_{i=1}^K \boldsymbol{u}_i^1}{||\sum_{i=1}^K \boldsymbol{u}_i^1||_2}, \quad \sigma_{top} = \frac{1}{K}\sum_{i=1}^K \sigma_i^1, \quad \boldsymbol{v}_{\text{top}} = \frac{\sum_{i=1}^K \boldsymbol{v}_i^1}{||\sum_{i=1}^K \boldsymbol{v}_i^1||_2}. \tag{11}$$

After extracting the aligned subspace, we need to retain the residual subspace of each specialised model with respect to the aligned subspace to preserve task-specific information. Specifically, we compute the rank-one matrices $\mathbf{M}_{\text{top}} = \sigma_{top}\boldsymbol{u}_{\text{top}}(\boldsymbol{v}_{\text{top}})^\top$ and $\mathbf{M}_i^1 = \sigma_i^1 \boldsymbol{u}_i^1(\boldsymbol{v}_i^1)^\top$. And then project $\mathbf{M}_i^1$ onto $\mathbf{M}_{\text{top}}$ to obtain the residual component $\mathbf{M}_{\text{res},i}$.

$$\mathbf{M}_{\text{res},i} = \mathbf{M}_i^1 - \text{Proj}_{\mathbf{M_{top}}}(\mathbf{M_i^1})\mathbf{M}_{\text{top}}. \tag{12}$$

Applying SVD on $\mathbf{M}_{\text{res},i}$ yields its top singular vectors and value: $\boldsymbol{u}_{\text{res},i}$, $\sigma_{\text{res},i}$ and $\boldsymbol{v}_{\text{res},i}$. We then concatenate $\boldsymbol{u}_{\text{top}}$, $\{\boldsymbol{u}_{\text{res},i}\}_{i=1}^K$ and $\{\boldsymbol{u}_i^r\}_{i=1}^K$ for subspaces from 2 to $L = (R-1)/K$ to construct $\hat{\mathbf{U}}$. The same procedure is applied to $\hat{\mathbf{\Sigma}}$ and $\hat{\mathbf{V}}$. The formal process is given as follows:

$$\hat{\mathbf{U}} = [\boldsymbol{u}_{\text{top}},\ \{\boldsymbol{u}_{\text{res},i}, \boldsymbol{u}_i^{2:L}\}_{i=1}^K], \hat{\mathbf{V}} = [\boldsymbol{v}_{\text{top}},\ \{\boldsymbol{v}_{\text{res},i}, \boldsymbol{v}_i^{2:L}\}_{i=1}^K], \hat{\mathbf{\Sigma}} = [\boldsymbol{\sigma}_{\text{top}},\ \{\boldsymbol{\sigma}_{\text{res},i}, \boldsymbol{\sigma}_i^{2:L}\}_{i=1}^K], \tag{13}$$

here $\boldsymbol{u}_i^{2:L}$ denotes the collection $\boldsymbol{u}_i^r$ for $r = 2, \ldots, L$, and similarly for the other terms. Following TSV-M (Gargiulo et al., 2025), we apply whitening to orthogonalise both $\hat{\mathbf{U}}$ and $\hat{\mathbf{V}}$ and obtain orthogonal bases $\hat{\mathbf{U}}_\perp$ and $\hat{\mathbf{V}}_\perp$. Specifically, we perform SVD on $\hat{\mathbf{U}}$ as $\hat{\mathbf{U}} = \mathbf{PDQ}^\top$, and set $\hat{\mathbf{U}}_\perp = \mathbf{PQ}^T$. The computation for $\hat{\mathbf{V}}_\perp$ is analogously.

Finally, we reconstruct the merged weight $\Delta\widetilde{\mathbf{W}}_{\text{merge}}$ using the singular vectors $\hat{\mathbf{u}}_\perp^r$ and $\hat{\mathbf{v}}_\perp^r$ from $\hat{\mathbf{U}}$ and $\hat{\mathbf{V}}$, respectively, and divide by η to ensure that the distance between the merged model and the individual models in the weight space is minimised. Pseudocode is provided in Algorithm 1.

$$\Delta\widetilde{\mathbf{W}}_{\text{merge}} = \sqrt{\frac{\sum_{r=1}^R (\hat{\sigma}^r)^2}{\sum_{r=1}^R (\hat{\sigma}^r/\eta^r)^2}} \sum_{r=1}^R \frac{\hat{\sigma}^r}{\eta^r}\, \hat{\mathbf{u}}_\perp^r(\hat{\mathbf{v}}_\perp^r)^\top. \tag{14}$$

When computing the final merged model, we additionally multiply by the factor $\sqrt{\frac{\sum_{r=1}^R (\hat{\sigma}^r)^2}{\sum_{r=1}^R (\hat{\sigma}^r/\eta^r)^2}}$ to ensure that the overall Frobenius norm of the weights remains consistent before and after scaling by η^r (Details in Appendix B.4). The final weights are then obtained by $\mathbf{W}_{\text{merge}} = \mathbf{W}_{\text{pre}} + \Delta\widetilde{\mathbf{W}}_{\text{merge}}$.

5 Experiments

5.1 Experimental Protocol

Baselines and Datasets. For empirical validation, we benchmark our method against several SOTA training-free model merging methods, including TA (Ilharco et al., 2022), TIES Yadav et al. (2023), DARE (Yu et al., 2024), TSV-M (Gargiulo et al., 2025) and Iso-C (Marczak et al., 2025a). All results are obtained from our own experiments under a unified evaluation protocol. As the checkpoints used here may differ from those in the original works, the reported performance may deviate from that in its original paper. Notably, current training-free methods have outperformed training-based methods like AdaMerging++ (Yang et al., 2024c) and Surgery (Yang et al., 2024b).

Consistent with prior studies Ilharco et al. (2022); Yang et al. (2024c), our primary experiments regard computer vision (CV) are conducted on 8 classification benchmarks, and primary experiments regard natural language processing (NLP) are conducted on 11 classification benchmarks and 2 open LLM Leaderboard. More detail can be found in Appendix.

Implementation Details. We use the ViT-B/32 CLIP model as the default visual encoder, consistent with the setup in Yang et al. (2024c). By default, the scaling coefficient $\lambda = 0.3$ for both Task Arithmetic (TA) and TIES-Merging (TIES), as recommended in their papers. For parameter pruning, TIES and DARE preserve the top 20% of the parameters. The hyperparameters introduced in AlignMerge-B can be selected based on the validation set, we use default values of $\alpha = 1.8$.

5.2 Vision & Language: Main Results

Computer Vision (CV) Experiments. Following prior work(Marczak et al., 2025a), we evaluate average classification accuracy across 8 and 14 datasets and show in Tab. 1 (Details are defer to Appendix E.1). Both AlignMerge-B and AlignMerge-O consistently achieve SOTA results in diverse merging tasks. In particular, the performance gap between AlignMerge-O and the empirical upper bound of traditional MTL methods (88.9 % for ViT-B/16) is reduced to only 3.6%.

Table 1: Consolidated average accuracy (%) across CV benchmarks. Per-dataset results are deferred to the appendix. Due to the use of different checkpoints, certain methods (*e.g.*, Iso-C and Iso-CTS) exhibit differently from reported in the original paper.

	8 Tasks			**14 Tasks**		
Method	**ViT-B/32**	**ViT-B/16**	**ViT-L/14**	**ViT-B/32**	**ViT-B/16**	**ViT-L/14**
Reference (non-merging)						
Pretrained	48.0	55.2	64.9	56.6	61.7	70.4
Individual	90.5	93.0	94.4	87.3	89.5	91.4
Training-free merging						
TA (Ilharco et al., 2022)	69.1	73.8	84.4	64.0	64.3	72.9
TIES (Yadav et al., 2023)	72.2	75.7	84.4	61.6	61.6	78.7
DARE (Yu et al., 2024)	65.8	71.5	79.4	63.9	67.2	76.5
TSV-M (Gargiulo et al., 2025)	84.0	87.3	91.5	76.4	77.0	86.1
Iso-C (Marczak et al., 2025a)	83.1	87.5	91.4	73.4	72.3	86.7
Iso-CTS (Marczak et al., 2025a)	81.4	86.9	90.9	76.7	79.2	**87.5**
AlignMerge-B (Ours)	84.9	88.5	**92.2**	76.8	77.4	86.5
AlignMerge-O (Ours)	**85.3**	**88.7**	92.1	**78.5**	**79.3**	86.8

Natural Language Processing (NLP) Experiments. We evaluate our method across NLP models of varying sizes in Table 2 (Details defer to Appendix E.1). AlignMerge achieves SOTA performance on both conventional small language models and recent large language models (LLMs). For T0, we follow Yu et al. (2024) and adopt IA^3-based Parameter-efficient fine-tuning (PEFT). Because IA^3 yields task vectors as vectors rather than full weight matrices, an SVD is not defined; consequently, SVD-dependent approaches (*e.g.*, TSV-M, Iso-C, AlignMerge-O) are not applicable, denoted as —.

Table 2: Consolidated performance across NLP benchmarks. Details are deferred to the appendix. Llama2 is evaluated on two generation benchmarks; others are used as encoders for classification.

	Generative Evaluation		**Encoder-derived Classification**		
Method	**Llama2-7B (FT)**		**BERT (FT)**	**T5 (FT)**	**T0 (PEFT)**
	AlphcaEval$\uparrow$	**GSM8K$\uparrow$**	**Avg Acc (%)**	**Avg Acc (%)**	**Avg Acc (%)**
TA (Ilharco et al., 2022)	42.6	43.8	67.0	41.5	62.2
TIES (Yadav et al., 2023)	40.3	45.0	64.3	41.2	62.8
DARE (Yu et al., 2024)	37.2	47.0	65.8	45.5	65.1
TSV-M (Gargiulo et al., 2025)	48.1	49.7	69.3	46.5	—
Iso-C (Marczak et al., 2025a)	29.5	42.0	63.7	43.9	—
Iso-CTS (Marczak et al., 2025a)	24.0	38.7	62.5	38.8	—
AlignMerge-B (Ours)	48.3	47.9	**70.6**	**50.0**	**65.9**
AlignMerge-O (Ours)	**88.1**	**51.0**	69.8	46.6	—

5.3 Empirical Analysis and Ablation Studies

Ablation Study. We ablate the sensitivity-control hyperparameter α in AlignMerge-B. As shown in Fig. 4, α thresholds the degree of subspace-alignment that triggers correction. Even with $\alpha = 0$ (no gating), AlignMerge-B consistently outperforms baselines such as TA. With proper tuning of α, AlignMerge-B delivers further gains and surpasses the current state of the art. However, setting α too high degrades performance because few subspaces are corrected. For unseen tasks, our empirical results suggest using $\alpha \approx \frac{1}{4}|\mathcal{T}|$ as a reasonable default, where $|\mathcal{T}|$ denotes the number of tasks.

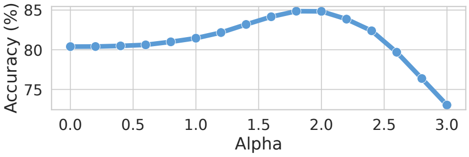

Figure 4: Ablation alpha on AlignMerge-B.

Table 3: Ablation study on AlignMerge-O.

Method	Removed component	Acc. (%)
AlignMerge-O	None	**85.32**
	w/o Alignment Extraction	85.11
	w/o Divide η	84.21
	w/o Both Components	83.99

For AlignMerge-O, which has no hyperparameters, we assess the contribution of each component in the setting with eight tasks (Tab. 3). The results show that the extraction of alignment subspaces and the normalization by η are both essential for effective model merging. Additional experiments are provided in Appendix E.2.

Preference Optimisation. AlignMerge-B can suppresses over-amplification of activations for specific tasks, thereby improving task-specific performance. We refer to this, which accentuates particular model performance post-merging, as Preference Optimisation. In Fig. 5, each cell at position (i, j) indicates the performance in task j after preference optimisation specifically for task i (with column-wise normalisation). The numbers in parentheses indicate the original classification accuracy. It can be observed that preference optimisation of AlignMerge-B typically yields high values for the diagonal elements in each column. Additionally, related tasks may benefit from this optimisation, while those with large domain differences may see degraded performance. For example, optimising for "Cars" improves performance on the natural image dataset "SUN397", whereas remote sensing ("EuroSAT") and digit recognition ("SVHN") tasks show limited gains.

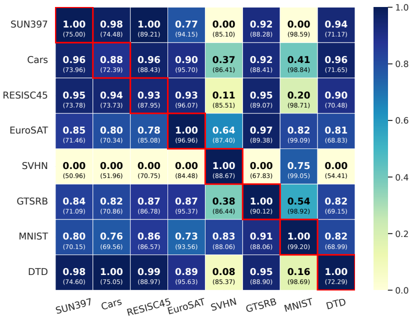

Figure 5: Merging performance target on 1 task.

Cost Analysis. Consistent with TSV-M and ISO-CTS, our method applies SVD to a selected subset of linear layers, which introduces additional cost. Even on 7B-parameter LLMs, this overhead is acceptable. Moreover, the overall cost is substantially lower than training-based multi-task learning (MTL), since no parameter updates are performed and the decompositions are computed once offline. Table 4 summarizes the runtime and peak memory footprint of AlignMerge-O across backbones.

Table 4: Additional runtime and memory usage caused by our merging across backbones.

Backbone	Time Cost	Memory Usage
ViT-B/32	131.4 s	8.21 MiB
ViT-B/16	130.9 s	8.21MiB
ViT-L/14	422.8 s	8.22MiB
LLaMA2 7B	1899.9s	8.19MiB

6 Conclusion

We revisit interference in model merging beyond conflict-only explanations. By analyzing weights across singular subspaces, we show that top singular subspaces exhibit strong alignment that induces activation over-amplification at inference and degrades performance. To address this, we introduce two independent strategies: AlignMerge-B, which applies subspace-aware rescaling after merging, and AlignMerge-O, which enforces subspace orthogonalization before merging while preserving aligned structure. Both approaches consistently mitigate over-alignment and achieve SOTA results across vision and language benchmarks, with especially strong gains on LLMs.

REFERENCES

MNIST handwritten digit database, Yann LeCun, Corinna Cortes and Chris Burges. https://yann.lecun.com/exdb/mnist/.

Emanuele Aiello, Lili Yu, Yixin Nie, Armen Aghajanyan, and Barlas Oguz. Jointly Training Large Autoregressive Multimodal Models, September 2023.

Tiago A. Almeida, José María G. Hidalgo, and Akebo Yamakami. Contributions to the study of SMS spam filtering: New collection and results. In Proceedings of the 11th ACM Symposium on Document Engineering, DocEng '11, pp. 259–262, New York, NY, USA, September 2011. Association for Computing Machinery. ISBN 978-1-4503-0863-2. doi: 10.1145/2034691.2034742.

Lukas Bossard, Matthieu Guillaumin, and Luc Van Gool. Food-101 – Mining Discriminative Components with Random Forests. In David Fleet, Tomas Pajdla, Bernt Schiele, and Tinne Tuytelaars (eds.), Computer Vision – ECCV 2014, volume 8694, pp. 446–461, Cham, 2014. Springer International Publishing. ISBN 978-3-319-10598-7 978-3-319-10599-4. doi: 10.1007/978-3-319-10599-4_29.

Gong Cheng, Junwei Han, and Xiaoqiang Lu. Remote Sensing Image Scene Classification: Benchmark and State of the Art. Proceedings of the IEEE, 105(10):1865–1883, October 2017. ISSN 1558-2256. doi: 10.1109/JPROC.2017.2675998.

Rajas Chitale, Ankit Vaidya, Aditya Kane, and Archana Ghotkar. Task Arithmetic with LoRA for Continual Learning, November 2023.

Mircea Cimpoi, Subhransu Maji, Iasonas Kokkinos, Sammy Mohamed, and Andrea Vedaldi. Describing Textures in the Wild. In Proceedings of the IEEE Conference on Computer Vision and Pattern Recognition, pp. 3606–3613, 2014.

Tarin Clanuwat, Mikel Bober-Irizar, Asanobu Kitamoto, Alex Lamb, Kazuaki Yamamoto, and David Ha. Deep Learning for Classical Japanese Literature, December 2018.

Adam Coates, Andrew Ng, and Honglak Lee. An Analysis of Single-Layer Networks in Unsupervised Feature Learning. In Proceedings of the Fourteenth International Conference on Artificial Intelligence and Statistics, pp. 215–223. JMLR Workshop and Conference Proceedings, June 2011.

Karl Cobbe, Vineet Kosaraju, Mohammad Bavarian, Mark Chen, Heewoo Jun, Lukasz Kaiser, Matthias Plappert, Jerry Tworek, Jacob Hilton, Reiichiro Nakano, Christopher Hesse, and John Schulman. Training verifiers to solve math word problems. arXiv preprint arXiv:2110.14168, 2021.

Gregory Cohen, Saeed Afshar, Jonathan Tapson, and André van Schaik. EMNIST: Extending MNIST to handwritten letters. In 2017 International Joint Conference on Neural Networks (IJCNN), pp. 2921–2926, May 2017. doi: 10.1109/IJCNN.2017.7966217.

Jasper Dekoninck, Marc Fischer, Luca Beurer-Kellner, and Martin Vechev. Controlled Text Generation via Language Model Arithmetic, March 2024.

Jacob Devlin, Ming-Wei Chang, Kenton Lee, and Kristina Toutanova. Bert: Pre-training of deep bidirectional transformers for language understanding. In Proceedings of the 2019 conference of the North American chapter of the association for computational linguistics: human language technologies, volume 1 (long and short papers), pp. 4171–4186, 2019.

Xibin Dong, Zhiwen Yu, Wenming Cao, Yifan Shi, and Qianli Ma. A survey on ensemble learning. Frontiers of Computer Science, 14(2):241–258, April 2020. ISSN 2095-2236. doi: 10.1007/s11704-019-8208-z.

Guodong Du, Junlin Lee, Jing Li, Runhua Jiang, Yifei Guo, Shuyang Yu, Hanting Liu, Sim K Goh, Ho-Kin Tang, Daojing He, et al. Parameter competition balancing for model merging. Advances in Neural Information Processing Systems, 37:84746–84776, 2024.

Guodong Du, Zitao Fang, Jing Li, Junlin Li, Runhua Jiang, Shuyang Yu, Yifei Guo, Yangneng Chen, Sim Kuan Goh, Ho-Kin Tang, et al. Neural parameter search for slimmer fine-tuned models and better transfer. arXiv preprint arXiv:2505.18713, 2025.

Li Fei-Fei, R. Fergus, and P. Perona. Learning Generative Visual Models from Few Training Examples: An Incremental Bayesian Approach Tested on 101 Object Categories. In 2004 Conference on Computer Vision and Pattern Recognition Workshop, pp. 178–178, June 2004. doi: 10.1109/CVPR.2004.383.

Antonio Andrea Gargiulo, Donato Crisostomi, Maria Sofia Bucarelli, Simone Scardapane, Fabrizio Silvestri, and Emanuele Rodolà. Task Singular Vectors: Reducing Task Interference in Model Merging, April 2025.

Charles Goddard, Shamane Siriwardhana, Malikeh Ehghaghi, Luke Meyers, Vlad Karpukhin, Brian Benedict, Mark McQuade, and Jacob Solawetz. Arcee's MergeKit: A Toolkit for Merging Large Language Models, March 2024.

Ian J. Goodfellow, Dumitru Erhan, Pierre Luc Carrier, Aaron Courville, Mehdi Mirza, Ben Hamner, Will Cukierski, Yichuan Tang, David Thaler, Dong-Hyun Lee, Yingbo Zhou, Chetan Ramaiah, Fangxiang Feng, Ruifan Li, Xiaojie Wang, Dimitris Athanasakis, John Shawe-Taylor, Maxim Milakov, John Park, Radu Ionescu, Marius Popescu, Cristian Grozea, James Bergstra, Jingjing Xie, Lukasz Romaszko, Bing Xu, Zhang Chuang, and Yoshua Bengio. Challenges in Representation Learning: A Report on Three Machine Learning Contests. In Minho Lee, Akira Hirose, Zeng-Guang Hou, and Rhee Man Kil (eds.), Neural Information Processing, pp. 117–124, Berlin, Heidelberg, 2013. Springer. ISBN 978-3-642-42051-1. doi: 10.1007/978-3-642-42051-1_16.

Yifei He, Yuzheng Hu, Yong Lin, Tong Zhang, and Han Zhao. Localize-and-Stitch: Efficient Model Merging via Sparse Task Arithmetic, August 2024.

Patrick Helber, Benjamin Bischke, Andreas Dengel, and Damian Borth. EuroSAT: A Novel Dataset and Deep Learning Benchmark for Land Use and Land Cover Classification. IEEE Journal of Selected Topics in Applied Earth Observations and Remote Sensing, 12(7):2217–2226, July 2019. ISSN 2151-1535. doi: 10.1109/JSTARS.2019.2918242.

Chenyu Huang, Peng Ye, Tao Chen, Tong He, Xiangyu Yue, and Wanli Ouyang. EMR-Merging: Tuning-Free High-Performance Model Merging, May 2024.

Gabriel Ilharco, Marco Tulio Ribeiro, Mitchell Wortsman, Ludwig Schmidt, Hannaneh Hajishirzi, and Ali Farhadi. Editing models with task arithmetic. In The Eleventh International Conference on Learning Representations, September 2022.

Pavel Izmailov, Dmitrii Podoprikhin, Timur Garipov, Dmitry Vetrov, and Andrew Gordon Wilson. Averaging Weights Leads to Wider Optima and Better Generalization, February 2019.

Xisen Jin, Xiang Ren, Daniel Preotiuc-Pietro, and Pengxiang Cheng. Dataless Knowledge Fusion by Merging Weights of Language Models, October 2023.

Jonathan Krause, Michael Stark, Jia Deng, and Li Fei-Fei. 3D Object Representations for Fine-Grained Categorization. In Proceedings of the IEEE International Conference on Computer Vision Workshops, pp. 554–561, 2013.

Alex Krizhevsky. Learning Multiple Layers of Features from Tiny Images.

Xuechen Li, Tianyi Zhang, Yann Dubois, Rohan Taori, Ishaan Gulrajani, Carlos Guestrin, Percy Liang, and Tatsunori B. Hashimoto. Alpacaeval: An automatic evaluator of instruction-following models. `https://github.com/tatsu-lab/alpaca_eval`, 5 2023.

Yayuan Li, Jintao Guo, Lei Qi, Wenbin Li, and Yinghuan Shi. Text and image are mutually beneficial: Enhancing training-free few-shot classification with clip. In Proceedings of the AAAI Conference on Artificial Intelligence, volume 39, pp. 5039–5047, 2025.

Haokun Liu, Derek Tam, Mohammed Muqeeth, Jay Mohta, Tenghao Huang, Mohit Bansal, and Colin A Raffel. Few-shot parameter-efficient fine-tuning is better and cheaper than in-context learning. Advances in Neural Information Processing Systems, 35:1950–1965, 2022.

Zhenyi Lu, Chenghao Fan, Wei Wei, Xiaoye Qu, Dangyang Chen, and Yu Cheng. Twin-Merging: Dynamic Integration of Modular Expertise in Model Merging, October 2024.

Haipeng Luo, Qingfeng Sun, Can Xu, Pu Zhao, Jianguang Lou, Chongyang Tao, Xiubo Geng, Qingwei Lin, Shifeng Chen, and Dongmei Zhang. Wizardmath: Empowering mathematical reasoning for large language models via reinforced evol-instruct. arXiv preprint arXiv:2308.09583, 2023.

Subhransu Maji, Esa Rahtu, Juho Kannala, Matthew Blaschko, and Andrea Vedaldi. Fine-Grained Visual Classification of Aircraft, June 2013.

Daniel Marczak, Simone Magistri, Sebastian Cygert, Bartłomiej Twardowski, Andrew D. Bagdanov, and Joost van de Weijer. No Task Left Behind: Isotropic Model Merging with Common and Task-Specific Subspaces, February 2025a.

Daniel Marczak, Bartłomiej Twardowski, Tomasz Trzciński, and Sebastian Cygert. MAGMAX: Leveraging Model Merging for Seamless Continual Learning. In Aleš Leonardis, Elisa Ricci, Stefan Roth, Olga Russakovsky, Torsten Sattler, and Gül Varol (eds.), Computer Vision – ECCV 2024, pp. 379–395, Cham, 2025b. Springer Nature Switzerland. ISBN 978-3-031-73013-9. doi: 10.1007/978-3-031-73013-9_22.

Michael S. Matena and Colin A. Raffel. Merging Models with Fisher-Weighted Averaging. Advances in Neural Information Processing Systems, 35:17703–17716, December 2022.

Yuval Netzer, Tao Wang, Adam Coates, Alessandro Bissacco, Bo Wu, and Andrew Y Ng. Reading Digits in Natural Images with Unsupervised Feature Learning.

Shiwen Ni, Dingwei Chen, Chengming Li, Xiping Hu, Ruifeng Xu, and Min Yang. Forgetting before Learning: Utilizing Parametric Arithmetic for Knowledge Updating in Large Language Models. In ACL (1), January 2024.

Maria-Elena Nilsback and Andrew Zisserman. Automated Flower Classification over a Large Number of Classes. In 2008 Sixth Indian Conference on Computer Vision, Graphics & Image Processing, pp. 722–729, December 2008. doi: 10.1109/ICVGIP.2008.47.

Changdae Oh, Yixuan Li, Kyungwoo Song, Sangdoo Yun, and Dongyoon Han. DaWin: Training-free Dynamic Weight Interpolation for Robust Adaptation. In The Thirteenth International Conference on Learning Representations, October 2024.

Guillermo Ortiz-Jimenez, Alessandro Favero, and Pascal Frossard. Task Arithmetic in the Tangent Space: Improved Editing of Pre-Trained Models. Advances in Neural Information Processing Systems, 36:66727–66754, December 2023.

Bo Pang and Lillian Lee. Seeing stars: Exploiting class relationships for sentiment categorization with respect to rating scales, June 2005.

Omkar M Parkhi, Andrea Vedaldi, Andrew Zisserman, and C. V. Jawahar. Cats and dogs. In 2012 IEEE Conference on Computer Vision and Pattern Recognition, pp. 3498–3505, June 2012. doi: 10.1109/CVPR.2012.6248092.

Colin Raffel, Noam Shazeer, Adam Roberts, Katherine Lee, Sharan Narang, Michael Matena, Yanqi Zhou, Wei Li, and Peter J Liu. Exploring the limits of transfer learning with a unified text-to-text transformer. Journal of machine learning research, 21(140):1–67, 2020.

Wei Ruan, Tianze Yang, Yifan Zhou, Tianming Liu, and Jin Lu. From Task-Specific Models to Unified Systems: A Review of Model Merging Approaches, March 2025.

Victor Sanh, Albert Webson, Colin Raffel, Stephen H Bach, Lintang Sutawika, Zaid Alyafeai, Antoine Chaffin, Arnaud Stiegler, Teven Le Scao, Arun Raja, et al. Multitask prompted training enables zero-shot task generalization. arXiv preprint arXiv:2110.08207, 2021.

Viraj Shah, Nataniel Ruiz, Forrester Cole, Erika Lu, Svetlana Lazebnik, Yuanzhen Li, and Varun Jampani. ZipLoRA: Any Subject in Any Style by Effectively Merging LoRAs. In Aleš Leonardis, Elisa Ricci, Stefan Roth, Olga Russakovsky, Torsten Sattler, and Gül Varol (eds.), Computer Vision – ECCV 2024, pp. 422–438, Cham, 2025. Springer Nature Switzerland. ISBN 978-3-031-73232-4. doi: 10.1007/978-3-031-73232-4_24.

Richard Socher, Alex Perelygin, Jean Wu, Jason Chuang, Christopher D. Manning, Andrew Ng, and Christopher Potts. Recursive Deep Models for Semantic Compositionality Over a Sentiment Treebank. In David Yarowsky, Timothy Baldwin, Anna Korhonen, Karen Livescu, and Steven Bethard (eds.), Proceedings of the 2013 Conference on Empirical Methods in Natural Language Processing, pp. 1631–1642, Seattle, Washington, USA, October 2013. Association for Computational Linguistics.

Johannes Stallkamp, Marc Schlipsing, Jan Salmen, and Christian Igel. The German Traffic Sign Recognition Benchmark: A multi-class classification competition. In The 2011 International Joint Conference on Neural Networks, pp. 1453–1460, July 2011. doi: 10.1109/IJCNN.2011.6033395.

George Stoica, Pratik Ramesh, Boglarka Ecsedi, Leshem Choshen, and Judy Hoffman. Model merging with SVD to tie the Knots, October 2024.

Wenju Sun, Qingyong Li, Wen Wang, Yangli-ao Geng, and Boyang Li. Task arithmetic in trust region: A training-free model merging approach to navigate knowledge conflicts. arXiv preprint arXiv:2501.15065, 2025.

Hugo Touvron, Louis Martin, Kevin Stone, Peter Albert, Amjad Almahairi, Yasmine Babaei, Nikolay Bashlykov, Soumya Batra, Prajjwal Bhargava, Shruti Bhosale, et al. Llama 2: Open foundation and fine-tuned chat models. arXiv preprint arXiv:2307.09288, 2023.

Bastiaan S. Veeling, Jasper Linmans, Jim Winkens, Taco Cohen, and Max Welling. Rotation Equivariant CNNs for Digital Pathology. In Alejandro F. Frangi, Julia A. Schnabel, Christos Davatzikos, Carlos Alberola-López, and Gabor Fichtinger (eds.), Medical Image Computing and Computer Assisted Intervention – MICCAI 2018, pp. 210–218, Cham, 2018. Springer International Publishing. ISBN 978-3-030-00934-2. doi: 10.1007/978-3-030-00934-2_24.

Fanqi Wan, Longguang Zhong, Ziyi Yang, Ruijun Chen, and Xiaojun Quan. FuseChat: Knowledge Fusion of Chat Models, August 2024.

Ke Wang, Nikolaos Dimitriadis, Guillermo Ortiz-Jimenez, François Fleuret, and Pascal Frossard. Localizing Task Information for Improved Model Merging and Compression, May 2024.

Alex Warstadt, Amanpreet Singh, and Samuel R. Bowman. Neural Network Acceptability Judgments. Transactions of the Association for Computational Linguistics, 7:625–641, September 2019. ISSN 2307-387X. doi: 10.1162/tacl_a_00290.

Mitchell Wortsman, Gabriel Ilharco, Samir Ya Gadre, Rebecca Roelofs, Raphael Gontijo-Lopes, Ari S. Morcos, Hongseok Namkoong, Ali Farhadi, Yair Carmon, Simon Kornblith, and Ludwig Schmidt. Model soups: Averaging weights of multiple fine-tuned models improves accuracy without increasing inference time. In Proceedings of the 39th International Conference on Machine Learning, pp. 23965–23998. PMLR, June 2022.

Han Xiao, Kashif Rasul, and Roland Vollgraf. Fashion-MNIST: A Novel Image Dataset for Benchmarking Machine Learning Algorithms, September 2017.

Jianxiong Xiao, Krista A. Ehinger, James Hays, Antonio Torralba, and Aude Oliva. SUN Database: Exploring a Large Collection of Scene Categories. International Journal of Computer Vision, 119 (1):3–22, August 2016. ISSN 0920-5691, 1573-1405. doi: 10.1007/s11263-014-0748-y.

Prateek Yadav, Derek Tam, Leshem Choshen, Colin A. Raffel, and Mohit Bansal. TIES-Merging: Resolving Interference When Merging Models. Advances in Neural Information Processing Systems, 36:7093–7115, December 2023.

Enneng Yang, Li Shen, Guibing Guo, Xingwei Wang, Xiaochun Cao, Jie Zhang, and Dacheng Tao. Model Merging in LLMs, MLLMs, and Beyond: Methods, Theories, Applications and Opportunities, September 2024a.

Enneng Yang, Li Shen, Zhenyi Wang, Guibing Guo, Xiaojun Chen, Xingwei Wang, and Dacheng Tao. Representation Surgery for Multi-Task Model Merging, May 2024b.

Enneng Yang, Zhenyi Wang, Li Shen, Shiwei Liu, Guibing Guo, Xingwei Wang, and Dacheng Tao. AdaMerging: Adaptive Model Merging for Multi-Task Learning, May 2024c.

Le Yu, Bowen Yu, Haiyang Yu, Fei Huang, and Yongbin Li. Language Models are Super Mario: Absorbing Abilities from Homologous Models as a Free Lunch. In Forty-First International Conference on Machine Learning, June 2024.

Chao Yuan, Tianyi Zhang, and Guanglin Niu. Neighbor-based feature and index enhancement for person re-identification. In Proceedings of the Computer Vision and Pattern Recognition Conference, pp. 5762–5769, 2025.

Xiang Zhang, Junbo Zhao, and Yann LeCun. Character-level Convolutional Networks for Text Classification. In Advances in Neural Information Processing Systems, volume 28. Curran Associates, Inc., 2015.

Zhenfei Zhang, Ming-Ching Chang, and Xin Li. Training-free image manipulation localization using diffusion models. In Proceedings of the AAAI Conference on Artificial Intelligence, volume 39, pp. 10376–10384, 2025.

Didi Zhu, Zhongyisun Sun, Zexi Li, Tao Shen, Ke Yan, Shouhong Ding, Chao Wu, and Kun Kuang. Model Tailor: Mitigating Catastrophic Forgetting in Multi-modal Large Language Models. In Forty-First International Conference on Machine Learning, June 2024.

A LLM Usage

We used a large language model solely as a writing assistant for copy-editing—improving grammar, wording, and clarity. The LLM did not generate or modify any technical content (ideas, algorithms, equations, proofs, experimental design, code, results, or figures). All scientific claims and analyses were conceived and written by the authors.

B Detailed Proof

B.1 Proof that the Projection for Rank-One Matrices Reduces to Singular Vector Projection.

The projection coefficient of $\mathbf{A}$ onto $\mathbf{B}$ in Frobenius inner product space is given by

$$\mathrm{Proj}_{\mathbf{B}}(\mathbf{A}) = \frac{\langle \mathbf{A}, \mathbf{B} \rangle_F}{\langle \mathbf{B}, \mathbf{B} \rangle_F} = \frac{\mathrm{tr}(\mathbf{A}^\top \mathbf{B})}{\|\mathbf{B}\|_F^2}. \tag{15}$$

Let $\mathbf{A} = \mathbf{a}_1 \mathbf{a}_2^\top \in \mathbb{R}^{m \times n}$ and $\mathbf{B} = \mathbf{b}_1 \mathbf{b}_2^\top \in \mathbb{R}^{m \times n}$ be two rank-one matrices, where $\mathbf{a}_1, \mathbf{b}_1 \in \mathbb{R}^m$ and $\mathbf{a}_2, \mathbf{b}_2 \in \mathbb{R}^n$. By substituting the forms of $\mathbf{A}$ and $\mathbf{B}$, we have

$$\mathbf{A}^\top \mathbf{B} = (\mathbf{a}_2 \mathbf{a}_1^\top)(\mathbf{b}_1 \mathbf{b}_2^\top) = \mathbf{a}_2 (\mathbf{a}_1^\top \mathbf{b}_1) \mathbf{b}_2^\top, \tag{16}$$

$$\mathrm{tr}(\mathbf{A}^\top \mathbf{B}) = (\mathbf{a}_1^\top \mathbf{b}_1)\, \mathrm{tr}(\mathbf{a}_2 \mathbf{b}_2^\top) = (\mathbf{a}_1^\top \mathbf{b}_1)(\mathbf{b}_2^\top \mathbf{a}_2). \tag{17}$$

Similarly,

$$\|\mathbf{B}\|_F^2 = \mathrm{tr}(\mathbf{B}^\top \mathbf{B}) = \mathrm{tr}\left((\mathbf{b}_2 \mathbf{b}_1^\top)(\mathbf{b}_1 \mathbf{b}_2^\top)\right) \tag{18}$$

$$= \mathrm{tr}\left(\mathbf{b}_2 (\mathbf{b}_1^\top \mathbf{b}_1) \mathbf{b}_2^\top\right) = (\mathbf{b}_1^\top \mathbf{b}_1)(\mathbf{b}_2^\top \mathbf{b}_2). \tag{19}$$

Therefore, the projection coefficient can be written as:

$$\mathrm{Proj}_{\mathbf{B}}(\mathbf{A}) = \frac{(\mathbf{a}_1^\top \mathbf{b}_1)(\mathbf{b}_2^\top \mathbf{a}_2)}{(\mathbf{b}_1^\top \mathbf{b}_1)(\mathbf{b}_2^\top \mathbf{b}_2)} = \frac{\langle \mathbf{a}_1, \mathbf{b}_1 \rangle}{\|\mathbf{b}_1\|^2} \cdot \frac{\langle \mathbf{a}_2, \mathbf{b}_2 \rangle}{\|\mathbf{b}_2\|^2} \tag{20}$$

That is, the projection coefficient of a rank-one matrix onto another rank-one matrix under the Frobenius inner product reduces to the product of the projection coefficients of their singular vectors.

B.2 Proof of Proposition 1.

Considering the relationship between the merged model $\Delta\mathbf{W}_{\text{merge}}$ and 2 specialised models $\Delta\mathbf{W}_i, \Delta\mathbf{W}_j$, we project $\Delta\mathbf{W}_j$ to assess its actual impact on task i:

$$\sigma^r_{\text{merge}}\mathbf{M}^r_{\text{merge}} = \eta^r\mathbf{P}^r_{\text{col}}\Delta\mathbf{W}_i\mathbf{P}^r_{\text{row}} + \eta^r\mathbf{P}^r_{\text{col}}\Delta\mathbf{W}_j\mathbf{P}^r_{\text{row}} \tag{21}$$

We begin by projecting $\mathbf{P}^r_{\text{col}}\boldsymbol{\Delta}\mathbf{W}^r_j$ onto the subspace spanned by $\mathbf{P}^r_{\text{col}}\boldsymbol{\Delta}\mathbf{W}^r_i$:

$$\mathbf{P}^r_{\text{col}}\,\boldsymbol{\Delta}\mathbf{W}^r_j\,\mathbf{P}^r_{\text{row}}\,\mathbf{x}_i = \alpha_1\,\mathbf{P}^r_{\text{col}}\,\boldsymbol{\Delta}\mathbf{W}^r_i\,\mathbf{P}^r_{\text{row}}\,\mathbf{x}_i + \mathbf{W}^r_{\text{res}}\,\mathbf{P}^r_{\text{row}}\,\mathbf{x}_i, \tag{22}$$

where $\alpha_1 = \text{Proj}_{\mathbf{P}^r_{\text{col}}\,\boldsymbol{\Delta}\mathbf{W}^r_i}\left(\mathbf{P}^r_{\text{col}}\,\boldsymbol{\Delta}\mathbf{W}^r_j\right)$, and $\mathbf{W}^r_{\text{res}}$ is the residual component orthogonal to $\mathbf{P}^r_{\text{col}}\boldsymbol{\Delta}\mathbf{W}^r_i$. Next, we project $\mathbf{W}^r_{\text{res}}\,\mathbf{P}^r_{\text{row}}$ onto the subspace spanned by $\mathbf{W}^r_i\,\mathbf{P}^r_{\text{row}}$:

$$\mathbf{W}^r_{\text{res}}\,\mathbf{P}^r_{\text{row}}\,\mathbf{x}_i = \alpha_2\,\mathbf{W}^r_i\,\mathbf{P}^r_{\text{row}}\,\mathbf{x}_i + \mathbf{W}^r_{\text{noise}}\,\mathbf{x}_i, \tag{23}$$

where $\alpha_2 = \text{Proj}_{\mathbf{W}^r_i\,\mathbf{P}^r_{\text{row}}}\left(\mathbf{W}^r_{\text{res}}\,\mathbf{P}^r_{\text{row}}\right)$, and $\mathbf{W}^r_{\text{noise}}$ is the final orthogonal residual.

Here, we estimate the total coefficient as

$$\xi^r_{i,j} = \alpha_1 + \alpha_2 \tag{24}$$

and the remaining residual $\epsilon^r_{i,j} = \mathbf{P}^r_{\text{col}}\,\mathbf{W}^r_{\text{noise}}$ as noise term. This leads to the expression in Proposition 1.

B.3 Proof of closed-form solution of the optimisation problem in Proposition 2.

We provide a proof for the closed-form solution to the optimisation problem stated in Proposition 2. The goal is to solve:

$$\min_{\boldsymbol{\Sigma}}\ \|\boldsymbol{\Delta}\mathbf{W}_i - \mathbf{S}\|_F^2, \quad \text{s.t.} \quad \mathbf{S} = \mathbf{U}_{\text{merge}}\,\boldsymbol{\Sigma}\,\mathbf{V}_{\text{merge}}, \ \ \boldsymbol{\Sigma} \text{ is diagonal.} \tag{25}$$

The objective function can be expanded as follows:

$$\begin{aligned} J(\boldsymbol{\Sigma}) &= \|\Delta\mathbf{W}_i - \mathbf{U}_{\text{merge}}\boldsymbol{\Sigma}\mathbf{V}_{\text{merge}}\|_F^2 && (26)\\ &= \text{trace}\left((\Delta\mathbf{W}_i - \mathbf{U}_{\text{merge}}\boldsymbol{\Sigma}\mathbf{V}_{\text{merge}})^\top(\Delta\mathbf{W}_i - \mathbf{U}_{\text{merge}}\boldsymbol{\Sigma}\mathbf{V}_{\text{merge}})\right) && (27)\\ &= \text{trace}(\Delta\mathbf{W}_i^\top\Delta\mathbf{W}_i) - 2\,\text{trace}(\boldsymbol{\Sigma}\mathbf{V}_{\text{merge}}\Delta\mathbf{W}_i^\top\mathbf{U}_{\text{merge}}) + \text{trace}(\boldsymbol{\Sigma}^\top\boldsymbol{\Sigma}). && (28) \end{aligned}$$

By defining $\boldsymbol{M} = \mathbf{U}_{\text{merge}}^\top\Delta\mathbf{W}_i\mathbf{V}_{\text{merge}}$, the objective simplifies to:

$$J(\boldsymbol{\Sigma}) = \text{const} - 2\,\text{trace}(\boldsymbol{\Sigma}^\top\boldsymbol{M}) + \text{trace}(\boldsymbol{\Sigma}^2). \tag{29}$$

Given that $\boldsymbol{\Sigma} = \text{diag}(\sigma_1, \sigma_2, \dots, \sigma_r)$ and $\boldsymbol{M} = [m_{ij}]$ with $m_{ii} = m_i$, the objective becomes:

$$J(\boldsymbol{\Sigma}) = \text{const} - 2\sum_i \sigma_i m_i + \sum_i \sigma_i^2. \tag{30}$$

Taking the derivative with respect to each σ_i and setting it to zero gives:

$$\frac{\partial J}{\partial \sigma_i} = -2m_i + 2\sigma_i = 0 \quad \Rightarrow \quad \sigma_i = m_i. \tag{31}$$

Thus, the optimal solution is:

$$\boldsymbol{\Sigma}^* = \text{diag}(\mathbf{U}_{\text{merge}}^\top\Delta\mathbf{W}_i\mathbf{V}_{\text{merge}}). \tag{32}$$

B.4 Proof that the Factor in Eq. 11 Ensures Frobenius Norm Invariance

We prove that the normalisation factor in Eq. 11 guarantees that the Frobenius norm remains invariant before and after scaling.

Let the original Frobenius norm of the weight matrix $\mathbf{W}$ be:

$$\|\mathbf{W}\|_F^2 = \sum_{r=1}^{R} (\sigma^r)^2. \tag{33}$$

After scaling the singular values σ^r by factors η^r, the new Frobenius norm becomes:

$$\left\| \sum_{r=1}^{R} \frac{\sigma^r}{\eta^r} \boldsymbol{u}_1^r (\boldsymbol{v}_1^r)^\top \right\|_F^2 = \sum_{r=1}^{R} \left(\frac{\sigma^r}{\eta^r} \right)^2. \tag{34}$$

To maintain the Frobenius norm, we introduce the normalisation factor: $\sqrt{\frac{\sum_{r=1}^{R} (\sigma^r)^2}{\sum_{r=1}^{R} \left(\frac{\sigma^r}{\eta^r}\right)^2}}$.

Thus, the Frobenius norm of the scaled weights is:

$$\left\| \widetilde{\mathbf{W}}_{\text{merge}} \right\|_F^2 = \left(\sqrt{\frac{\sum_{r=1}^{R} (\sigma^r)^2}{\sum_{r=1}^{R} \left(\frac{\sigma^r}{\eta^r}\right)^2}} \right)^2 \cdot \sum_{r=1}^{R} \left(\frac{\sigma^r}{\eta^r} \right)^2 = \sum_{r=1}^{R} (\sigma^r)^2. \tag{35}$$

Therefore, the normalisation factor ensures that the Frobenius norm of the weights remains unchanged after scaling, thereby preserving the representational capacity of the merged model.

C Pseudocode of AlignMerge-O

We provide the pseudocode for AlignMerge-O, where the intermediate orthogonalisation steps are similar to those in TSV-M (Gargiulo et al., 2025). The detailed pseudocode is shown in Algorithm 1.

D Additional Implementation Setting

Datasets. Consistent with prior studies Ilharco et al. (2022); Yang et al. (2024c), our primary experiments are conducted on 8 image classification benchmarks with various domain shift: SUN397 Xiao et al. (2016), Cars Krause et al. (2013), RESISC45 Cheng et al. (2017), EuroSAT Helber et al. (2019), SVHN Netzer et al., GTSRB Stallkamp et al. (2011), MNIST MNI, and DTD Cimpoi et al. (2014). To further demonstrate the versatility of our method, we extend our evaluation to some additional datasets: Caltech101 Fei-Fei et al. (2004), CIFAR10 Krizhevsky, CIFAR100 Krizhevsky, FGVC Maji et al. (2013), Flowers102 Nilsback & Zisserman (2008), Food101 Bossard et al. (2014), OxfordPets Parkhi et al. (2012), STL10 Coates et al. (2011), PCAM Veeling et al. (2018), FER2013 Goodfellow et al. (2013), EMNIST Cohen et al. (2017), FashionMNIST Xiao et al. (2017), RenderedSST2 Socher et al. (2013) and KMNIST Clanuwat et al. (2018). We fine-tune BERT on four binary classification datasets: AG News (Zhang et al., 2015), Rotten Tomatoes (Pang & Lee, 2005), CoLA (Warstadt et al., 2019), and SMS (Almeida et al., 2011). The resulting models are merged into a unified model using model merging techniques and evaluated on each task individually. TA and TIES use default settings, while TSV-M and AlignMerge-O are applied exclusively to BERT's most critical linear layer ("output.dense.weight"). Finally, to evaluate the performance of the merged model on LLMs, the fine-tuned models WizardMath-7B-V1.0 (Luo et al., 2023) and Llama-2-7b-chat-hf (Touvron et al., 2023) are merged and tested on two benchmarks, AlpacaEval (Li et al., 2023) and GSM8K (Cobbe et al., 2021).

Datasets License. Datasets distributed under the MIT License include: SVHN Netzer et al., STL10 Coates et al. (2011), EMNIST Cohen et al. (2017), FashionMNIST Xiao et al. (2017), and KMNIST Clanuwat et al. (2018).

Datasets released under various Creative Commons licenses consist of: EuroSAT Helber et al. (2019), DTD Cimpoi et al. (2014), RESISC45 Cheng et al. (2017), Food101 Bossard et al. (2014)

Algorithm 1: AlignMerge through orthogonalisation (AlignMerge-O)

```
Input: Pretrained weight $\Delta\mathbf{W}_{\text{pre}}$ and $K$ task-specific weights $\Delta\mathbf{W}_1, \ldots, \Delta\mathbf{W}_K$
Output: Merged model weight $\mathbf{W}_{\text{merge}}$
for $i = 1$ to $K$ do
    Compute SVD: $\Delta\mathbf{W}_i = \mathbf{U}_i\mathbf{\Sigma}_i\mathbf{V}_i^\top = \sum_{r=1}^{R} \sigma_i^r \boldsymbol{u}_i^r(\boldsymbol{v}_i^r)^\top = \sum_{r=1}^{R} \sigma_i^r \mathbf{M}_i^r$ ;
    Retain top $\frac{R-1}{K}$ singular components of $\mathbf{U}_i$, $\mathbf{\Sigma}_i$, and $\mathbf{V}_i$;
Extract the aligned subspace: ;
$\boldsymbol{u}_{\text{top}} = \frac{\sum_{i=1}^{K} \boldsymbol{u}_i^1}{||\sum_{i=1}^{K} \boldsymbol{u}_i^1||_2}$, $s_{top} = \frac{1}{K}\sum_{i=1}^{K} s_i^1$, $\boldsymbol{v}_{\text{top}} = \frac{\sum_{i=1}^{K} \boldsymbol{v}_i^1}{||\sum_{i=1}^{K} \boldsymbol{v}_i^1||_2}$ ;
$\mathbf{M}_{\text{top}} = \sigma_{top}\boldsymbol{u}_{\text{top}}(\boldsymbol{v}_{\text{top}})^\top$;
Compute the residual component: ;
for $i = 1$ to $K$ do
    $\mathbf{M}_i^1 = \sigma_i^1 \boldsymbol{u}_i^1(\boldsymbol{v}_i^1)^\top$ ;
    $\mathbf{M}_{\text{res},i} = \mathbf{M}_i^1 - \left(\text{Proj}_{\mathbf{M}_{\mathbf{top}}^{\mathbf{1}}}(\mathbf{M}_i^1)\right)\mathbf{M}_{\text{top}}$ ;
    Retain only main component in $\mathbf{M}_{\textbf{res},i}$: ;
    $\mathbf{M}_{\text{res},i} = \mathbf{U}_{\text{res},i}\mathbf{\Sigma}_{\text{res},i}(\mathbf{V}_{\text{res},i})^\top = \sum_{r=1}^{R} \sigma_{\text{res},i}^r \boldsymbol{u}_{\text{res},i}^r(\boldsymbol{v}_{\text{res},i}^r)^\top$,;
Concatenate the matrices: ;
    $\hat{\mathbf{U}} = \left[\boldsymbol{u}_{\text{top}},\ \{\boldsymbol{u}_{\text{res},i}^1\}_{i=1}^K,\ \{\boldsymbol{u}_i^{2:(R-1)/K}\}_{i=1}^K\right]$ ;
    $\hat{\mathbf{\Sigma}} = \left[\boldsymbol{\sigma}_{\text{top}},\ \{\boldsymbol{\sigma}_{\text{res},i}^1\}_{i=1}^K,\ \{\boldsymbol{\sigma}_i^{2:(R-1)/K}\}_{i=1}^K\right]$ ;
    $\hat{\mathbf{V}} = \left[\boldsymbol{v}_{\text{top}},\ \{\boldsymbol{v}_{\text{res},i}^1\}_{i=1}^K,\ \{\boldsymbol{v}_i^{2:(R-1)/K}\}_{i=1}^K\right]$ ;
Compute the SVD of $\hat{\mathbf{U}}$ and $\hat{\mathbf{V}}$: ;
$\hat{\mathbf{U}} = \mathbf{P}_U\mathbf{D}_U\mathbf{Q}_U^\top$;
$\hat{\mathbf{V}} = \mathbf{P}_V\mathbf{D}_V\mathbf{Q}_V^\top$;
Obtain the orthogonal matrices: ;
$\hat{\mathbf{U}}_\perp = \mathbf{P}_U\mathbf{Q}_U^\top = [\hat{\boldsymbol{u}}_\perp^1, \hat{\boldsymbol{u}}_\perp^2, \ldots, \hat{\boldsymbol{u}}_\perp^R]$;
$\hat{\mathbf{V}}_\perp = \mathbf{P}_V\mathbf{Q}_V^\top = [\hat{\boldsymbol{v}}_\perp^1, \hat{\boldsymbol{v}}_\perp^2, \ldots, \hat{\boldsymbol{v}}_\perp^R]$;
for $r = 1$ to $R$ do
    $\eta^r = \hat{\sigma}^r / \left((\hat{\boldsymbol{u}}_\perp^r)^\top \sum_{i=1}^{K} \Delta\mathbf{W}_i\hat{\boldsymbol{v}}_\perp^r\right)$
Reconstruct the merged matrix: ;
$\Delta\widetilde{\mathbf{W}}_{\text{merge}} = \sqrt{\frac{\sum_{r=1}^{R}(\hat{\sigma}^r)^2}{\sum_{r=1}^{R}(\hat{\sigma}^r/\eta^r)^2}} \sum_{r=1}^{R} \frac{\hat{\sigma}^r}{\eta^r} \hat{\boldsymbol{u}}_\perp^r(\hat{\boldsymbol{v}}_\perp^r)^\top$;
Construct merged model weights: ;
$\mathbf{W}_{\text{merge}} = \mathbf{W}_{\text{pre}} + \Delta\widetilde{\mathbf{W}}_{\text{merge}}$;
return $\mathbf{W}_{\text{merge}}$ ;
```

The following datasets are available strictly for non-commercial research or academic use, typically under custom or restrictive academic licenses: SUN397 Xiao et al. (2016), Cars Krause et al. (2013), GTSRB Stallkamp et al. (2011), FGVC Maji et al. (2013), Flowers102 Nilsback & Zisserman (2008), OxfordPets Parkhi et al. (2012), Caltech101 Fei-Fei et al. (2004), FER2013 Goodfellow et al. (2013), PCAM Veeling et al. (2018), and RenderedSST2 Socher et al. (2013).

The MNIST MNI and CIFAR10/100 Krizhevsky datasets are provided for unrestricted research use and are considered to be in the public domain or distributed without explicit license restrictions.

For full details regarding dataset licenses and terms of use, please refer to the official web pages or documentation of the respective datasets.

Implementation Detail. All experiments are conducted using PyTorch on a single NVIDIA GeForce A800 GPU. Following prior work (Ilharco et al., 2022; Yadav et al., 2023), the value of α can be selected via the validation set: $\alpha = 0.6$ for two-model merging tasks, $\alpha = 2.8$ for fourteen-model tasks, and $\alpha = 6.5$ for twenty-model tasks.

E Experiments

Here, we present experiments that were not included in the main paper due to space limitations.

E.1 Experiments Details

Merging experiments on 8 CV benchmark The performance of each method on individual datasets is presented in detail. Complete results for ViT-B/32, ViT-B/16, and ViT-L/14 are provided in Table 5, Table 6, and Table 7, respectively.

Method	SUN397.	Cars.	RESISC45.	EuroSAT.	SVHN.	GTSRB.	MNIST.	DTD.	Avg Acc.
Pretrained	62.3	59.7	60.7	45.5	31.4	32.6	48.5	43.8	48.1
Individual	75.3	77.7	96.1	99.7	97.5	98.7	99.7	79.4	90.5
Traditional MTL	73.9	74.4	93.9	98.2	95.8	98.9	99.5	77.9	89.1
TA	64.7	63.3	71.4	72.7	64.2	52.8	87.5	50.1	65.8
DARE	64.8	63.5	71.8	72.4	63.8	52.4	87.5	50.5	65.8
TIES	59.6	58.6	71.0	81.3	86.1	70.9	98.4	54.7	72.6
TSVM	69.1	70.7	85.5	94.3	92.0	91.9	99.3	69.2	84.0
ISO-C	74.8	74.1	87.9	92.9	83.1	86.0	98.2	67.9	83.1
ISO-CTS	74.4	74.4	87.2	90.4	76.8	83.3	97.4	67.0	81.4
AlignMerge-B	73.7	73.8	88.8	95.6	86.7	89.7	98.9	71.5	84.8
AlignMerge-O	72.0	74.2	86.9	94.7	91.0	92.7	99.2	71.8	**85.3**

Table 5: Performance comparison across different methods and 8 datasets on ViT-B/32.

Method	SUN397.	Cars.	RESISC45.	EuroSAT.	SVHN.	GTSRB.	MNIST.	DTD.	Avg Acc.
Pretrained	63.8	64.7	66.4	54.6	52.0	43.4	51.7	44.7	55.2
Individual	81.8	86.8	96.9	99.8	97.9	99.2	99.8	82.1	93.0
TA	61.1	65.9	74.0	76.2	88.0	73.9	98.4	53.0	73.8
DARE	67.6	70.0	76.1	78.6	75.3	59.8	94.4	50.1	71.5
TIES	59.1	72.5	80.5	84.0	85.0	71.5	98.1	54.9	75.7
TSVM	72.8	80.4	89.1	96.6	93.9	93.9	99.3	72.7	87.3
ISO-C	78.1	82.3	91.9	96.9	88.3	91.9	98.8	71.9	87.5
ISO-CTS	77.9	83.2	92.1	96.4	84.9	91.3	98.4	71.1	86.9
AlignMerge-B	76.3	81.0	91.7	97.6	92.1	94.2	99.1	75.8	88.5
AlignMerge-O	75.4	82.9	90.7	98.0	93.0	95.0	99.2	75.6	**88.7**

Table 6: Performance comparison across different methods and 8 datasets on ViT-B/16.

Method	SUN397.	Cars.	RESISC45.	EuroSAT.	SVHN.	GTSRB.	MNIST.	DTD.	Avg Acc.
Pretrained	66.9	77.9	71.3	62.2	58.5	50.6	76.4	55.4	64.9
Individual	84.9	92.4	97.4	99.7	98.1	99.2	99.7	84.2	94.4
TA	74.0	81.9	86.5	92.9	87.8	86.8	99.0	66.1	84.4
DARE	71.1	81.6	82.6	90.6	78.3	70.8	97.0	63.1	79.4
TIES	74.4	84.5	88.0	94.0	85.7	82.1	98.7	67.7	84.4
TSVM	79.1	89.9	94.0	98.9	95.3	96.2	99.5	79.1	91.5
ISO-C	81.9	90.9	94.8	98.7	91.4	95.5	99.2	79.2	91.4
ISO-CTS	81.3	91.2	94.7	98.6	89.4	95.3	99.2	77.9	90.9
AlignMerge-B	82.2	90.7	94.9	98.6	93.7	96.8	99.4	81.5	**92.2**
AlignMerge-O	79.9	90.8	94.7	98.9	95.1	96.7	99.5	80.9	92.1

Table 7: Performance comparison across different methods and 8 datasets on ViT-L/14.

Merging experiments on 14 CV benchmark The performance of each method on individual datasets is presented in detail. Complete results for ViT-B/32, ViT-B/16, and ViT-L/14 are provided in Table 8, Table 9, and Table 10, respectively.

Merging experiments on full fine-tuned BERT The performance of each method on individual datasets is presented in detail. Complete results for BERT (Devlin et al., 2019) are provided in Table 11.

Merging experiments on full fine-tuned T5 The performance of each method on individual datasets is presented in detail. Complete results for T5 (Raffel et al., 2020) are provided in Table 12.

Merging experiments on PEFT fine-tuned T0 The detailed performance of each method on individual datasets is provided. IA3 (Liu et al., 2022) is employed for model Parameter-Efficient

Method	Caltech101	Cars	CIFAR100	DTD	EuroSAT	FGVC	Flowers102	Food101	GTSRB	MNIST	OxfordPets	RESISC45	SUN397	SVHN	Avg. Acc.
Pretrained	89.2	59.6	66.1	44.4	45.7	17.0	73.5	79.5	32.6	48.3	82.3	60.3	62.3	31.6	56.6
Individual	95.1	77.7	89.3	79.4	99.8	46.6	87.3	85.0	98.7	99.7	90.5	96.1	79.2	97.5	87.3
TA	91.4	62.4	72.0	46.8	64.8	18.6	73.5	78.9	44.0	76.9	85.1	67.0	63.5	51.6	64.0
DARE	91.6	62.4	71.7	46.7	64.3	18.5	73.5	78.9	43.7	76.7	85.1	67.0	63.6	51.4	63.9
TIES	86.6	55.9	69.7	47.1	70.6	30.0	49.0	65.1	53.0	87.7	69.8	63.5	59.0	55.1	61.6
TSVM	90.8	67.0	74.3	65.5	94.6	37.1	60.8	73.9	88.4	99.0	86.7	81.0	64.1	86.9	76.4
ISO-C	91.2	63.9	75.5	61.2	90.9	39.0	50.0	69.2	83.6	98.5	78.8	77.5	65.5	82.7	73.4
ISO-CTS	92.7	68.7	77.1	64.9	89.8	39.2	64.7	75.5	85.8	98.5	83.4	82.8	68.7	82.4	76.7
AlignMerge-B	91.8	71.0	81.2	66.3	92.2	38.1	61.8	77.7	81.8	97.5	85.1	84.1	70.7	75.7	76.8
AlignMerge-O	91.4	68.7	75.8	67.5	94.3	39.8	68.6	77.9	89.3	99.0	87.8	83.4	68.0	87.7	78.5

Table 8: Performance comparison across different methods and 14 datasets on ViT-B/32.

Method	Caltech101	Cars	CIFAR100	DTD	EuroSAT	FGVC	Flowers102	Food101	GTSRB	MNIST	OxfordPets	RESISC45	SUN397	SVHN	Avg. Acc.
Pretrained	86.7	64.7	69.6	44.7	54.6	25.1	67.7	85.7	43.4	51.7	87.2	66.4	63.8	52.0	61.7
Individual	97.4	86.8	89.7	82.0	99.8	54.7	82.4	90.3	99.1	99.8	94.6	96.8	81.7	97.8	89.5
TA	87.6	65.9	73.0	45.9	60.1	26.3	67.6	85.6	46.6	64.4	85.9	68.7	64.9	57.3	64.3
DARE	88.5	66.0	75.8	46.2	66.1	26.3	67.6	83.8	50.6	86.3	83.7	70.4	65.6	64.0	67.2
TIES	89.8	53.7	80.2	38.4	50.9	26.9	54.9	75.5	40.6	87.7	85.6	56.8	59.4	61.5	61.6
TSVM	90.2	69.9	77.9	54.7	91.6	35.3	66.7	81.5	85.7	98.8	92.9	80.2	64.4	88.5	77.0
ISO-C	94.4	51.7	79.5	46.1	85.1	35.4	57.8	75.9	79.0	98.4	92.9	73.3	58.8	84.3	72.3
ISO-CTS	93.7	71.3	77.0	58.8	93.8	39.6	74.5	80.9	90.8	98.9	93.8	81.4	65.8	89.3	79.2
AlignMerge-B	94.4	68.8	81.7	54.6	88.9	37.4	69.6	82.9	83.0	98.2	92.0	80.8	65.2	85.5	77.4
AlignMerge-O	90.6	73.6	78.2	59.2	93.0	39.2	72.5	83.3	88.0	98.8	94.0	83.5	66.9	89.0	79.3

Table 9: Performance comparison across different methods and 14 datasets on ViT-B/16.

Method	Caltech101	Cars	CIFAR100	DTD	EuroSAT	FGVC	Flowers102	Food101	GTSRB	MNIST	OxfordPets	RESISC45	SUN397	SVHN	Avg. Acc.
Pretrained	91.4	77.9	78.5	55.4	62.3	31.5	81.4	89.6	50.5	76.3	93.8	71.3	66.9	58.4	70.4
Individual	95.8	92.3	87.8	84.1	99.7	65.0	88.2	92.6	99.2	99.7	94.3	97.4	84.9	98.1	91.4
TA	91.8	78.9	80.0	56.8	68.7	32.4	82.4	89.7	54.7	84.2	94.0	74.3	67.7	64.3	72.9
DARE	91.8	79.8	82.0	59.5	81.4	32.3	84.3	89.6	62.4	93.2	94.6	78.6	69.4	71.8	76.5
TIES	93.5	78.3	79.1	61.4	88.0	30.9	83.3	85.4	73.2	98.1	93.8	83.6	71.4	81.8	78.7
TSVM	93.8	88.2	80.3	74.5	98.1	39.3	92.2	89.4	95.2	99.4	94.3	91.7	74.6	94.0	86.1
ISO-C	93.8	89.0	82.3	74.2	97.4	42.8	92.2	90.0	94.7	99.3	95.4	93.2	78.3	91.2	86.7
ISO-CTS	94.1	90.3	83.2	76.3	98.3	42.6	93.1	91.4	95.7	99.3	95.4	94.2	78.7	91.8	87.5
AlignMerge-B	93.8	89.1	83.6	73.8	97.0	42.5	92.2	90.3	93.1	99.1	95.1	94.0	78.3	89.5	86.5
AlignMerge-O	93.8	89.4	81.1	75.4	98.4	40.5	94.1	90.3	96.0	99.5	94.8	92.8	75.4	94.2	86.8

Table 10: Performance comparison across different methods and 14 datasets on ViT-L/14.

Method	Ag_news	Rotten_Tomatoes	Cola	SMS	Avg. Acc.
TA	94.2	51.0	33.8	89.1	67.0
TIES	88.7	47.0	41.5	79.9	64.3
DARE	90.8	50.8	33.9	87.5	65.8
TSVM	97.9	52.4	34.8	91.9	69.3
ISO-C	77.2	44.7	40.7	92.3	63.7
ISO-CTS	73.2	43.6	42.9	90.1	62.5
AlignMerge-O	97.4	53.4	36.4	92.1	69.8
AlignMerge-B	97.8	59.9	34.4	90.3	**70.6**

Table 11: Performance comparison across different methods and datasets on BERT.

Method	rte	cb	winogrande	wic	wsc	copa	h-swag	story_cloze	anli-r1	anli-r2	anli-r3	Avg. Acc.
TA	40.6	53.1	34.4	60.9	37.5	48.4	21.9	50.0	34.4	40.6	34.4	41.5
DARE	40.6	53.1	31.2	59.4	37.5	50.0	21.9	50.0	34.4	40.6	34.4	41.2
TIES	40.6	56.2	34.4	71.9	37.5	68.8	21.9	59.4	34.4	43.8	31.2	45.5
TSVM	43.8	71.9	40.6	57.8	37.5	59.4	25.0	68.8	34.4	40.6	31.2	46.5
ISO-C	40.6	68.8	37.5	57.8	37.5	50.0	28.1	59.4	34.4	40.6	28.1	43.9
ISO-CTS	40.6	53.1	37.5	42.2	39.1	48.4	25.0	43.8	31.2	37.5	28.1	38.8
AlignMerge-O	42.2	75.0	50.0	51.6	37.5	56.2	28.1	65.6	34.4	40.6	31.2	46.6
AlignMerge-B	43.8	68.8	34.4	62.5	37.5	60.9	28.1	65.6	34.4	40.6	34.4	46.5

Table 12: Performance comparison across different methods and tasks on T5.

Fine-Tuning (PEFT). AlignMerge-B† indicates that the model is first merged using the TIES method, followed by the proposed subspace calibration approach. Experimental results demonstrate that AlignMerge-B† achieves significantly better outcomes, highlighting the advantage of jointly addressing interference through the integration of conflict and alignment. Complete results for T0 (Sanh et al., 2021) are provided in Table 13, Where methods rely on SVD (*e.g.*, TSVM, Iso-C, AlignMerge-O) are not applicable.

Merging experiments on full fine-tuned Llama2 to evaluate the performance of the merged model on LLMs, the fine-tuned models WizardMath-7B-V1.0 (Luo et al., 2023) and Llama-2-7b-chat-hf (Touvron et al., 2023) are merged and tested on two benchmarks, AlpacaEval (Li et al., 2023) and GSM8K (Cobbe et al., 2021). Complete results for Llama2-7B (Touvron et al., 2023) are provided in Table 14.

Method	rte	cb	winogrande	wic	wsc	copa	h-swag	story_cloze	anli-r1	anli-r2	anli-r3	Avg. Acc.
TA	89.1	62.5	53.1	51.6	50	87.5	50	93.8	56.2	46.9	43.8	62.2
DARE	89.1	62.5	56.2	53.1	50	89.1	50	93.8	56.2	46.9	43.8	62.8
TIES	84.4	84.4	53.1	56.2	53.1	84.4	43.8	90.6	59.4	53.1	53.1	65.1
TSVM	–	–	–	–	–	–	–	–	–	–	–	–
Iso-c	–	–	–	–	–	–	–	–	–	–	–	–
Iso-CTS	–	–	–	–	–	–	–	–	–	–	–	–
AlignMerge-O	–	–	–	–	–	–	–	–	–	–	–	–
AlignMerge-B	71.9	81.2	59.4	68.8	43.8	93.8	50	93.8	56.2	46.9	59.4	65.9
AlignMerge-B†	82.8	93.8	65.6	70.4	54.6	81.2	46.9	90.6	62.5	56.2	62.5	69.7

Table 13: Performance comparison across different methods and tasks on T0.

Method	AlphcaEval (win_rate)	GSM8K (Acc. %)	Avg.
Task Arithmetic	42.6	43.8	43.2
TIES	40.3	45.0	42.7
DARE	37.2	47.0	42.1
TSV-M	48.1	49.7	48.9
ISO-C	29.5	42.0	35.7
ISO-CTS	24.0	38.7	31.4
AlignMerge_B (ours)	48.3	47.9	48.1
AlignMerge_O (ours)	88.1	51.0	69.6

Table 14: Performance comparison across different methods on Llama2-7B.

E.2 Additional Experiments

Existence of alignment across different backbone. In Fig. 1(b), we visualize subspace-alignment for ViT-B/32. To assess its prevalence, we additionally report ViT-L/14 and Llama2-7B in Fig. 6. For readability, we display only the top-32 singular subspaces. Across backbones, alignment is consistently concentrated in the top singular subspaces. Although the absolute scores for Llama2-7B seems are smaller, reflecting its larger matrix scale, the alignment pattern remains clear and pronounced.

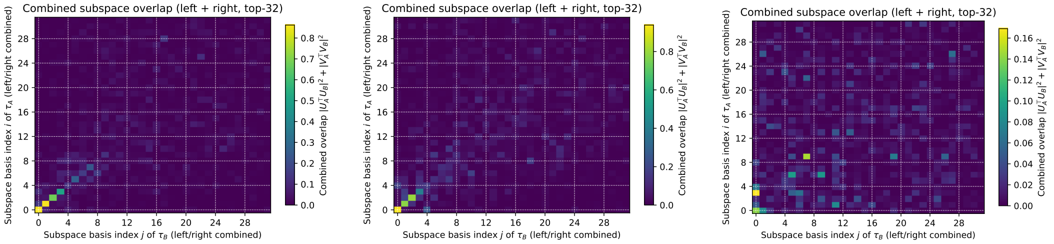

Figure 6: Visualisation of subspace-alignment (by subspace-overlap score) for the first linear layer of **ViT-B/16** (Left), **ViT-L/14** (Middle) and **Llama2-7B** (right).

Statistical Analysis. Since our method does not involve any randomness, we evaluate its effectiveness from a statistical perspective by constructing model merging tasks using random combinations of eight datasets from the main experiments, covering various numbers of models. We compare our AlignMerge-O method with TSVM in Fig. 9a, the results show that after conducting hundreds of experiments across different combinations, AlignMerge-O consistently outperforms the SOTA method.

Order of Column and Row Projection. In computing the Subspace Cross-Influence $\xi^r_{i,j}$, the paper adopts the default order of projecting onto the column subspace first, followed by projecting the residual onto the row subspace. However, this order is not mandatory. As shown in Fig. 7, we compute the coefficients in different singular vector subspaces of a random weight matrix. The results demonstrate that projecting onto the row subspace first and then onto the column subspace yields very similar coefficients.

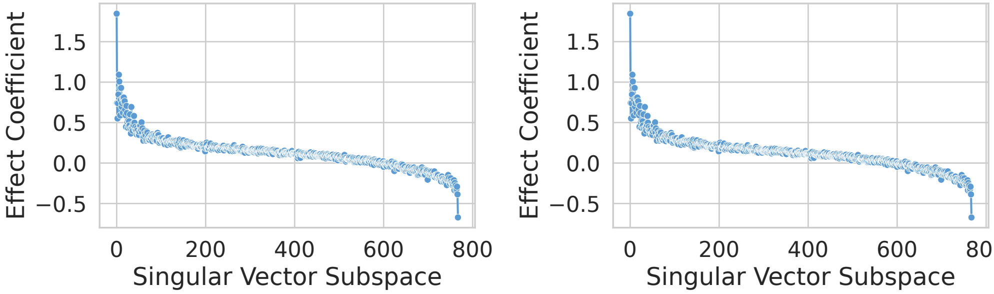

Figure 7: Visualisation of the Subspace Cross-Influence: the left shows projection onto the column subspace first, while the right shows projection onto the row subspace first.

Experiments with Varying Numbers of Datasets. As subspace-alignment are highly consistent across different models (shown in Fig. 6). Therefore, to demonstrate generalizability and reduce computational cost, for merging tasks involving more than 8 datasets, we use scaled coefficients derived from the eight-task scenario. Tab. 19 and Fig. 8 present results for fourteen- and twenty-task merging scenarios. Tab. 16 reports results for two-task merging, where eight tasks are randomly paired and the average accuracy across all pairs is indicated as ”Avg Acc.”. Fig. 9a further examines arbitrary combinations among the eight dataset models. These experiments collectively demonstrate that our method consistently yields robust improvements in varying scenarios.

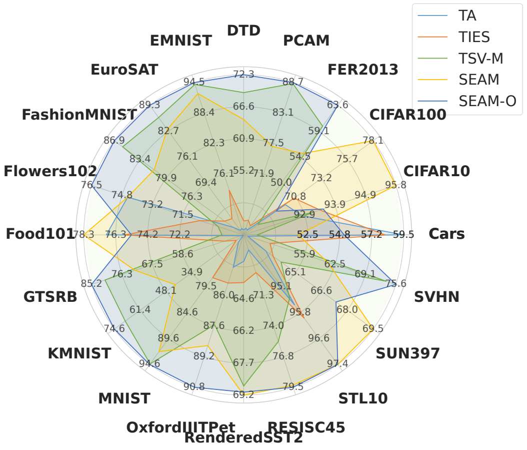

Figure 8: Merging performance on 20 tasks

The Universality of AlignMerge-B. In the main text, our AlignMerge-B method applies singular vector subspace correction after summing all weights. However, since subspace-alignment are prevalent in models produced by various merging methods, AlignMerge-B can also be effectively integrated into methods such as TIES (Yadav et al., 2023) and DARE (Yu et al., 2024). As shown in Tab. 15, we modify TIES-Merging by dividing each subspace of the merged model by its corresponding Subspace Cross-Influence, resulting in TIES w/ AlignMerge-B. The hyperparameters α are set the same as in the main paper. The results demonstrate that AlignMerge-B remains highly effective when applied to TIES, and the same holds for DARE w/ AlignMerge-B. With further tuning of these hyperparameters, performance is expected to improve even more.

Table 15: Applying AlignMerge-B on different merging methods.

Method	SUN397.	Cars.	RESISC45.	EuroSAT.	SVHN.	GTSRB.	MNIST.	DTD.	Avg Acc
TIES	59.6	58.59	70.96	81.33	86.14	70.85	98.36	54.73	72.57
TIES w/ AlignMerge-B	70.36	66.72	81.73	88.93	79.93	68.14	97.53	64.52	77.23
DARE	64.75	63.3	71.38	72.67	64.17	52.74	87.37	50.27	65.83
DARE w/ AlignMerge-B	64.91	65.07	79.75	93.04	89.92	84.77	99.08	61.28	79.73

Robustness On Unseen Tasks. Here, we evaluate zero-shot performance by merging models trained on 7 out of 8 datasets and testing on the remaining one. As shown in Fig. 9b, our AlignMerge-O consistently outperforms the SOTA TSV-M method in various scenarios.

Alignment of Singular Vector Subspace. As observed in the main text, the top singular vector subspaces of different task vectors exhibit high alignment. Here, we visualise the specific alignment between different singular vector subspaces. Specifically, we perform SVD on the task vectors of specialised models and extract the top-K singular vectors. By taking the outer product of the left and right singular vectors, we obtain a rank-1 matrix $\mathbf{M}_i$ for task i. We quantify the alignment between

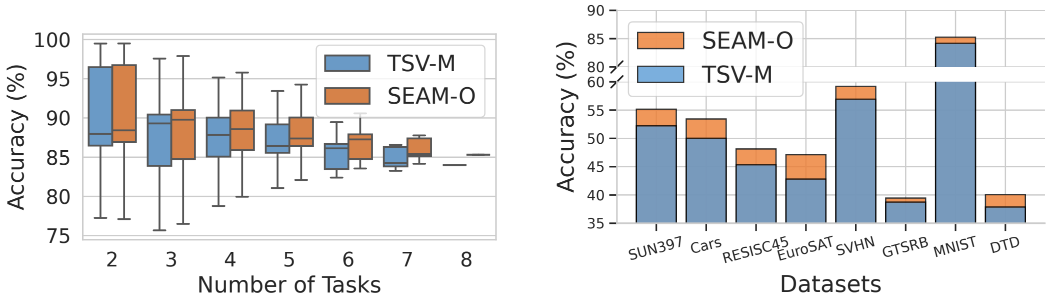

(a) Statistical analysis.

(b) Zero-shot performance.

Figure 9: Additional experiments (a) Statistical analysis based on arbitrary combinations of different models. (b) Evaluating the robustness on unseen tasks.

tasks i and j in the K-th singular vector subspace by computing $||\mathbf{M}_i^\top \mathbf{M}_j||_F$. Since both $\mathbf{M}_i$ and $\mathbf{M}_j$ are rank-1 matrices, $||\mathbf{M}_i^\top \mathbf{M}_j||_F = 1$ when they are identical, and $||\mathbf{M}_i^\top \mathbf{M}_j||_F = 0$ when they are orthogonal. The visualisation is shown in Fig. 10. Notably, the alignment between singular vector subspaces decreases from top-1 to top-4, and stabilises near zero beyond the top-4 subspace. This highlights the necessity of explicitly extracting the top-1 subspace in AlignMerge-O to prevent information loss due to orthogonalisation.

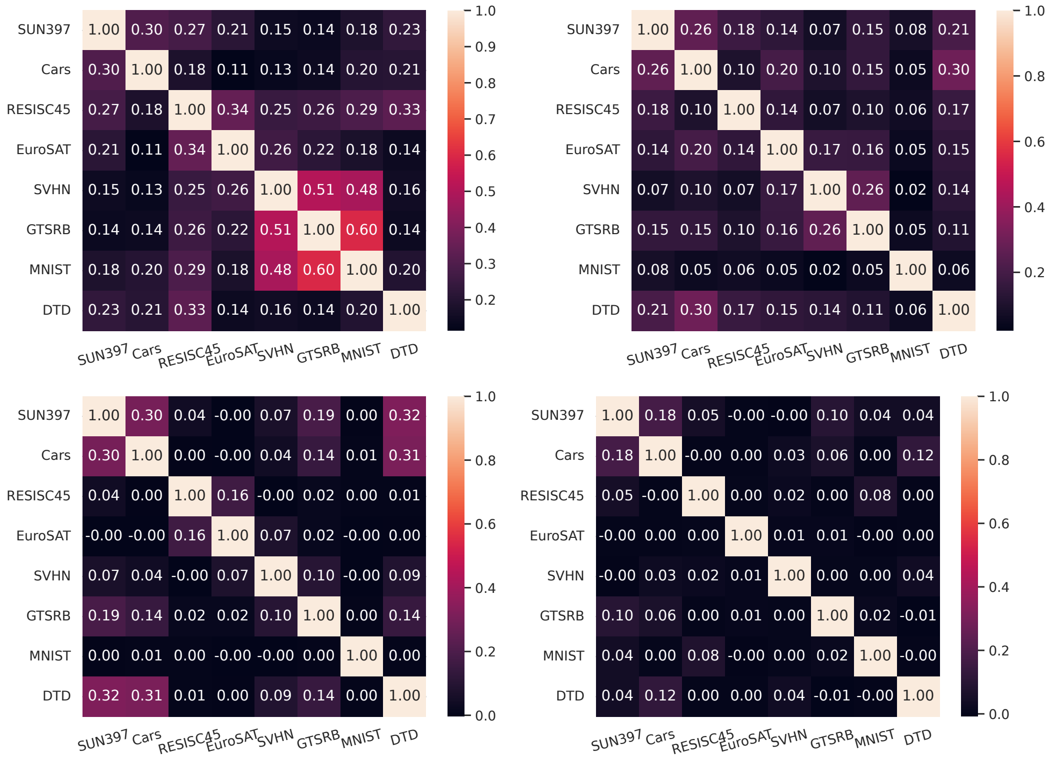

	SUN397	Cars	RESISC45	EuroSAT	SVHN	GTSRB	MNIST	DTD
SUN397	1.00	0.30	0.27	0.21	0.15	0.14	0.18	0.23
Cars	0.30	1.00	0.18	0.11	0.13	0.14	0.20	0.21
RESISC45	0.27	0.18	1.00	0.34	0.25	0.26	0.29	0.33
EuroSAT	0.21	0.11	0.34	1.00	0.26	0.22	0.18	0.14
SVHN	0.15	0.13	0.25	0.26	1.00	0.51	0.48	0.16
GTSRB	0.14	0.14	0.26	0.22	0.51	1.00	0.60	0.14
MNIST	0.18	0.20	0.29	0.18	0.48	0.60	1.00	0.20
DTD	0.23	0.21	0.33	0.14	0.16	0.14	0.20	1.00

	SUN397	Cars	RESISC45	EuroSAT	SVHN	GTSRB	MNIST	DTD
SUN397	1.00	0.26	0.18	0.14	0.07	0.15	0.08	0.21
Cars	0.26	1.00	0.10	0.20	0.10	0.15	0.05	0.30
RESISC45	0.18	0.10	1.00	0.14	0.07	0.10	0.06	0.17
EuroSAT	0.14	0.20	0.14	1.00	0.17	0.16	0.05	0.15
SVHN	0.07	0.10	0.07	0.17	1.00	0.26	0.02	0.14
GTSRB	0.15	0.15	0.10	0.16	0.26	1.00	0.05	0.11
MNIST	0.08	0.05	0.06	0.05	0.02	0.05	1.00	0.06
DTD	0.21	0.30	0.17	0.15	0.14	0.11	0.06	1.00

	SUN397	Cars	RESISC45	EuroSAT	SVHN	GTSRB	MNIST	DTD
SUN397	1.00	0.30	0.04	-0.00	0.07	0.19	0.00	0.32
Cars	0.30	1.00	0.00	-0.00	0.04	0.14	0.01	0.31
RESISC45	0.04	0.00	1.00	0.16	-0.00	0.02	0.00	0.01
EuroSAT	-0.00	-0.00	0.16	1.00	0.07	0.02	-0.00	0.00
SVHN	0.07	0.04	-0.00	0.07	1.00	0.10	-0.00	0.09
GTSRB	0.19	0.14	0.02	0.02	0.10	1.00	0.00	0.14
MNIST	0.00	0.01	0.00	-0.00	-0.00	0.00	1.00	0.00
DTD	0.32	0.31	0.01	0.00	0.09	0.14	0.00	1.00

	SUN397	Cars	RESISC45	EuroSAT	SVHN	GTSRB	MNIST	DTD
SUN397	1.00	0.18	0.05	-0.00	-0.00	0.10	0.04	0.04
Cars	0.18	1.00	-0.00	0.00	0.03	0.06	0.00	0.12
RESISC45	0.05	-0.00	1.00	0.00	0.02	0.00	0.08	0.00
EuroSAT	-0.00	0.00	0.00	1.00	0.01	0.01	-0.00	0.00
SVHN	-0.00	0.03	0.02	0.01	1.00	0.00	0.00	0.04
GTSRB	0.10	0.06	0.00	0.01	0.00	1.00	0.02	-0.01
MNIST	0.04	0.00	0.08	-0.00	0.00	0.02	1.00	-0.00
DTD	0.04	0.12	0.00	0.00	0.04	-0.01	-0.00	1.00

Figure 10: Visualisation of Singular Vector Subspace-Alignment. (Top left: Top-1 singular vector subspace; top right: Top-2; bottom left: Top-3; bottom right: Top-4)

Effectiveness of η. When modelling the relationship between the merged model and the specialized models, we introduce a scalar η to ensure equality (Eq. 4). In AlignMerge-B, we define $\eta^r = \sigma^r_{\text{merge}} / \left((\boldsymbol{u}^r_{\text{merge}})^\top \sum_{i=1}^{K} \Delta \mathbf{W}_i \boldsymbol{v}^r_{\text{merge}} \right)$. Whereas in AlignMerge-O, we define $\eta^r = \sigma^r_{\text{merge}} / \left((\boldsymbol{u}^r_{\text{merge}})^\top \Delta \mathbf{W}_{i^*} \boldsymbol{v}^r_{\text{merge}} \right)$, ensuring the singular values on both sides of the equation are exactly matched. Here, we visualise the singular values of the merged model obtained by AlignMerge-B, TIES w/ AlignMerge-B and AlignMerge-O, as well as the singular values obtained by directly projecting the specialised models onto the corresponding subspaces (Fig. 11). We observe that without η, the two singular values exhibit an approximately linear relationship. In AlignMerge-B, both singular values are exactly equal. In TIES w/ AlignMerge-B and AlignMerge-O, direct projection of the specialised models leads to singular values that are either excessively large or small compared to those of the merged model, respectively. Therefore, the absence of η significantly increases the distance between the merged and specialized models in weight space.

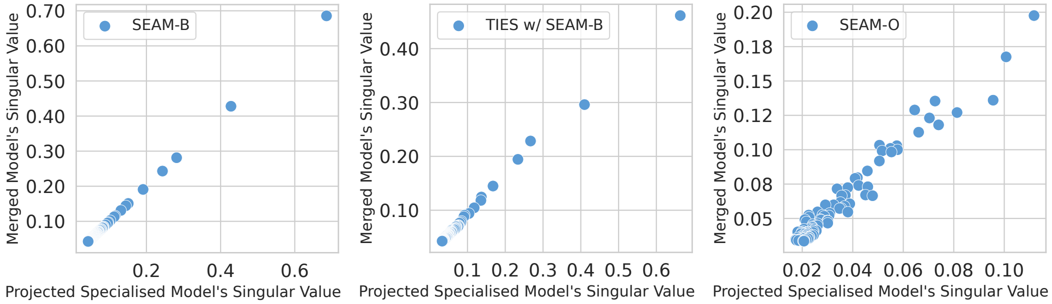

Figure 11: Visualisation of the singular values of the merged model compared to those of the projected specialised models.

Table 16: Multi-task performance (%) when merging ViT-B/32 models on random 2 task combinations. Combinations are: (EuroSAT, SUN397), (MNIST, DTD), (RESISC45, GTSRB), and (SVHN, Cars).

Method	EuroSAT	SUN397	MNIST	DTD	RESISC45	GTSRB	SVHN	Cars	Avg Acc
TA	98.8	73.8	99.5	69.3	91.1	95.3	95.4	72.0	86.9
TIES	98.7	75.1	99.6	71.1	92.8	95.6	96.3	73.8	87.9
TSV-M	99.8	76.6	99.7	76.8	94.4	98.4	97.3	74.8	89.7
AlignMerge-B	99.5	77.5	99.6	78.2	94.8	98.0	96.3	76.2	90.0
AlignMerge-O	99.5	77.5	99.6	77.1	95.1	98.2	96.9	76.7	**90.1**

F Relationship to Related Works

Current model merging methods can be broadly classified into static (Yu et al., 2024; He et al., 2024; Gargiulo et al., 2025) and dynamic methods (Huang et al., 2024; Yang et al., 2024b; Oh et al., 2024), with ours falling into the static category. The primary distinction lies in whether the model behaviour changes during inference for different inputs. In terms of space complexity, static methods typically require $\mathcal{O}(1)$ space, while dynamic methods require $\mathcal{O}(N)$, where N is the number of tasks. Although dynamic merging methods generally offer better performance, they often require prior knowledge of the input dataset and cannot allow the model to perform multiple tasks simultaneously. As a result, they are unsuitable for important applications such as style mixture in image generation.

In addition, model merging methods can also be divided into training-required (Yang et al., 2024c;b) and training-free (Ilharco et al., 2022; Yadav et al., 2023) methods, with ours belonging to the training-free category. Training-required methods typically rely on large amounts of unlabeled data—often using unlabeled test samples—for unsupervised training via entropy minimisation, which incurs high computational and data costs. Nevertheless, some training-free methods also depend on additional data resources; for example, DaWin (Oh et al., 2024) requires substantial unlabeled data, while TA (Ilharco et al., 2022) and TIES (Yadav et al., 2023) require validation sets to tune scaling coefficients for task vectors. Therefore, in this work, we mainly compare with static methods that are easily applicable in practice and rely only on a validation set. Notably, our SEAM-O can operate entirely without any additional data.

Table 17: Multi-task performance (%) when merging ViT-B/32 models on eight tasks.

Method	SUN397	Cars	RESISC45	EuroSAT	SVHN	GTSRB	MNIST	DTD	Avg Acc
Pretrained	62.3	59.7	60.7	45.5	31.4	32.6	48.5	43.8	48.0
Individual	75.3	77.7	96.1	99.7	97.5	98.7	99.7	79.4	90.5
Traditional MTL	73.9	74.4	93.9	98.2	95.8	98.9	99.5	77.9	88.9
Weight Averaging	65.3	63.4	71.4	71.7	64.2	52.8	87.5	50.1	65.8
TA	55.2	54.9	66.7	78.9	80.2	69.7	97.3	50.4	69.1
DARE	64.9	63.5	71.8	72.4	63.8	52.4	87.5	50.5	65.8
TIES	59.8	58.6	70.7	79.7	86.2	72.1	98.3	54.2	72.4
TSV-M	69.1	70.7	85.5	94.3	92.0	91.9	99.3	69.2	84.0
Iso-CTS	74.4	74.4	87.2	90.4	76.8	83.3	97.4	67.0	81.4
AlignMerge-B	73.8	73.8	88.8	95.7	86.7	89.7	98.9	71.5	84.9
AlignMerge-O	72.0	74.2	86.9	94.7	91.0	92.7	99.2	71.8	**85.3**

Table 18: Multi-task performance (%) when merging models with different backbones on 8 tasks.

Backbone	Method	SUN397	Cars	RESISC45	EuroSAT	SVHN	GTSRB	MNIST	DTD	Avg Acc
ViT-B/16	TA	61.1	65.9	74.0	76.2	88.0	73.9	98.4	53.0	73.8
	TIES	59.1	72.5	80.5	84.0	85.0	71.5	98.1	54.9	77.0
	TSV-M	72.8	80.4	89.1	96.6	93.9	93.9	99.3	72.7	87.3
	AlignMerge-B	76.3	81	91.7	97.6	92.1	94.2	99.1	75.8	88.5
	AlignMerge-O	75.4	82.9	90.7	98.0	93.0	95.0	99.2	75.6	**88.8**
ViT-L/14	TA	74.0	81.9	86.5	92.9	87.8	86.8	99.0	66.1	84.4
	TIES	74.4	84.5	88.0	94.0	85.7	82.1	98.7	67.7	84.4
	TSV-M	79.1	89.9	94.0	98.9	95.3	96.2	99.5	79.1	91.5
	AlignMerge-B	82.2	90.7	94.9	98.6	93.7	96.8	99.4	81.5	**92.2**
	AlignMerge-O	79.9	90.8	94.7	98.9	95.1	96.7	99.5	80.9	92.1

Table 19: Multi-task performance (%) when merging ViT-B/32 models on 14 tasks.

Method	Caltech101	Cars	CIFAR100	DTD	EuroSAT	FGVC	Flowers102	Food101	GTSRB	MNIST	OxfordPets	RESISC45	SUN397	SVHN	Avg Acc.
TA	91.4	62.4	72	46.8	64.8	18.6	73.5	78.9	44	76.9	85.1	67	63.5	51.6	64.0
TIES	86.6	55.9	69.7	47.1	70.6	30.0	49.0	65.1	53.0	87.7	69.8	63.5	59.0	55.1	61.6
TSV-M	90.8	67.0	74.3	65.5	94.6	37.1	60.8	73.9	88.4	99.0	86.7	81.0	64.1	86.9	76.4
AlignMerge-B	91.8	71.0	81.2	66.3	92.2	38.1	61.8	77.7	81.8	97.5	85.1	84.2	70.7	75.7	76.8
AlignMerge-O	91.4	68.7	75.8	67.5	94.3	39.8	68.6	77.9	89.3	99.0	87.8	83.4	68.0	87.7	**78.5**

G Detailed Visualisation

We paired models trained on each of the eight datasets in our main experiments and visualised the subspace-alignment across different layers for each pair. Experimental results are presented in Figs. 12, 13, 14, 15, and 16. The results indicate that while effect coefficients exhibit similar overall patterns across different pairs, notable differences remain; moreover, subspace-alignment generally dominate over conflict effects.

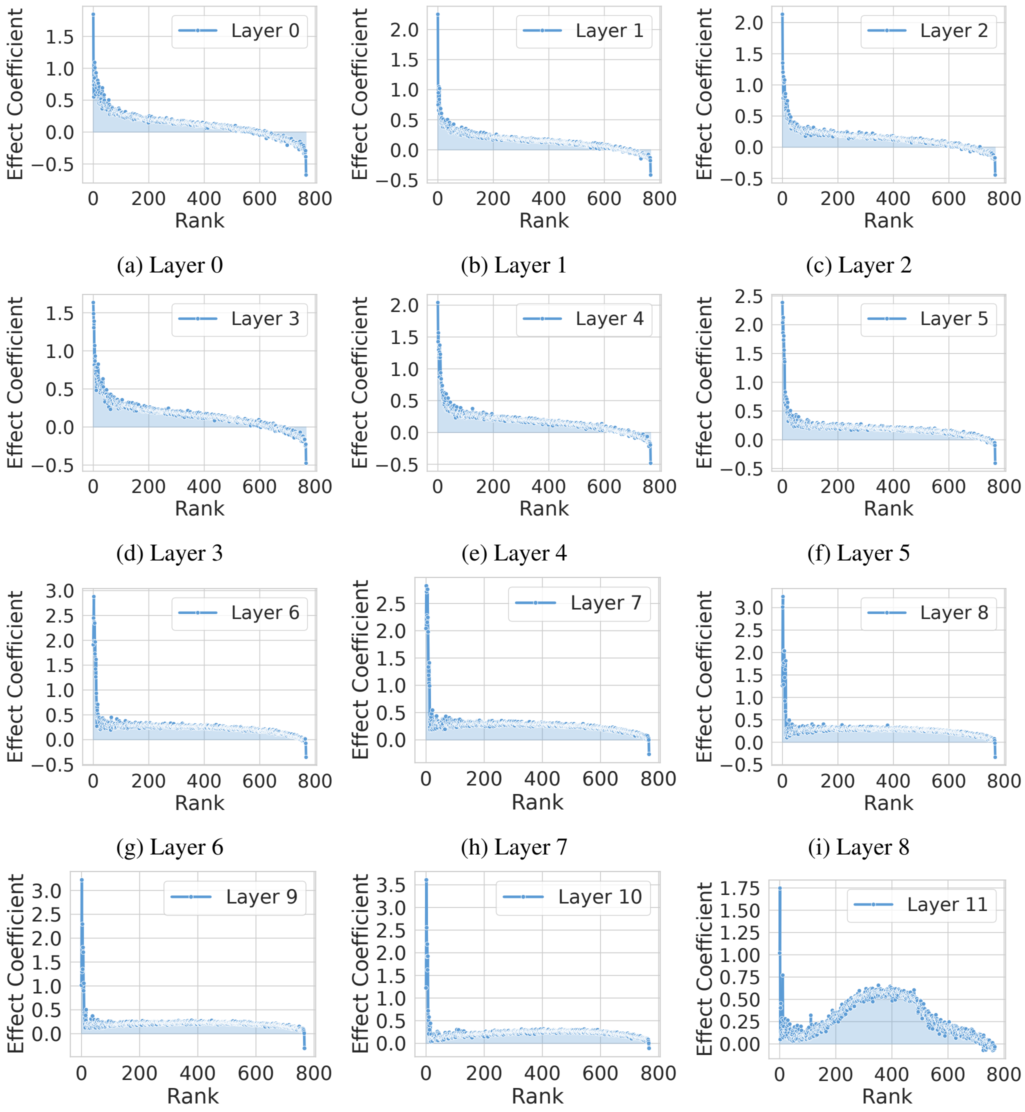

(a) Layer 0

(b) Layer 1

(c) Layer 2

(d) Layer 3

(e) Layer 4

(f) Layer 5

(g) Layer 6

(h) Layer 7

(i) Layer 8

(j) Layer 9

(k) Layer 10

(l) Layer 11

Figure 12: Subspace Cross-Influence that “MNIST” impact on “Cars” for all layers.

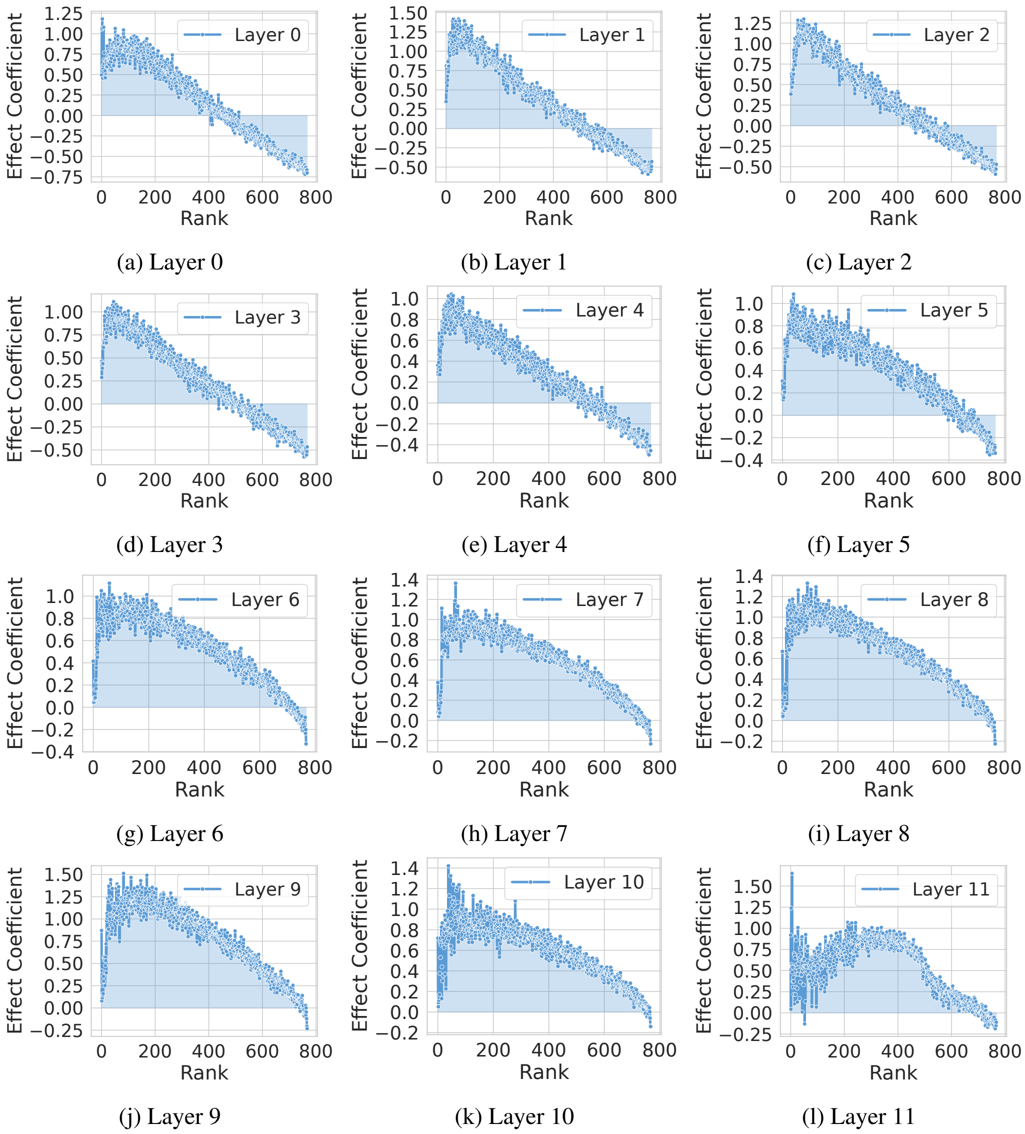

(a) Layer 0

(b) Layer 1

(c) Layer 2

(d) Layer 3

(e) Layer 4

(f) Layer 5

(g) Layer 6

(h) Layer 7

(i) Layer 8

(j) Layer 9

(k) Layer 10

(l) Layer 11

Figure 13: Subspace Cross-Influence that “Cars” impact on “MNIST” for all layers.

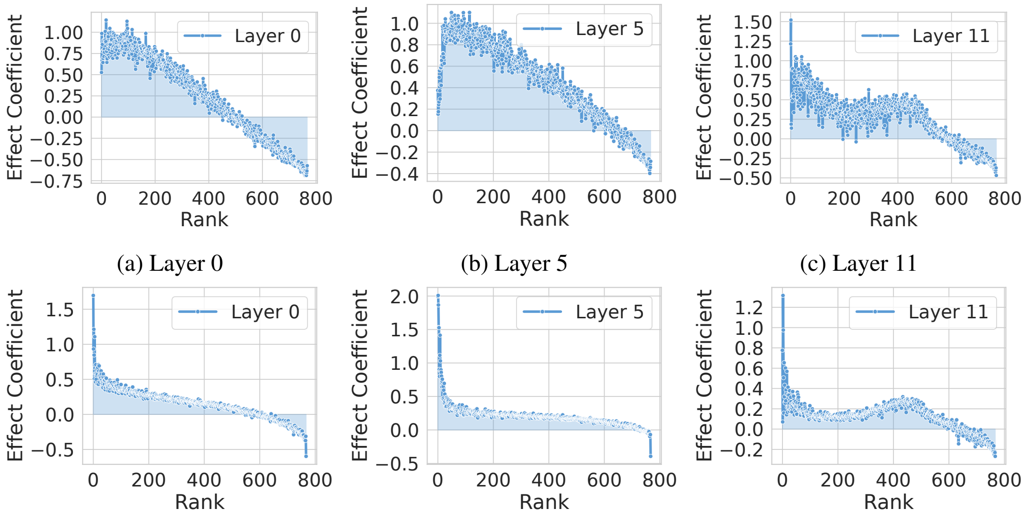

(a) Layer 0

(b) Layer 5

(c) Layer 11

(d) Layer 0

(e) Layer 5

(f) Layer 11

Figure 14: Subspace Cross-Influence that "SUN397" impact on "GTSRB" at first row and "GTSRB" impact on "SUN397" at second row.

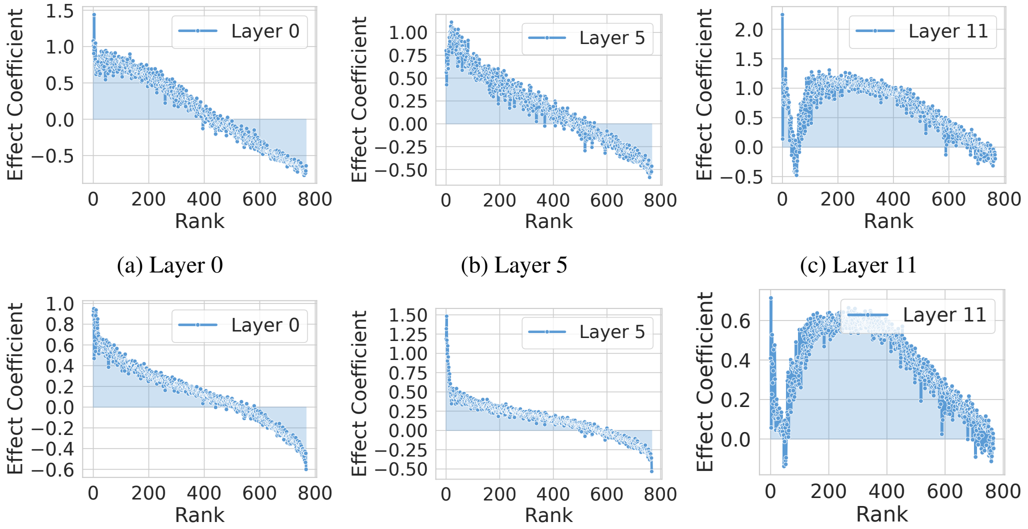

(a) Layer 0

(b) Layer 5

(c) Layer 11

(d) Layer 0

(e) Layer 5

(f) Layer 11

Figure 15: Subspace Cross-Influence that "RESISC45" impact on "EuroSAT" at first row and "EuroSAT" impact on "RESISC45" at second row.

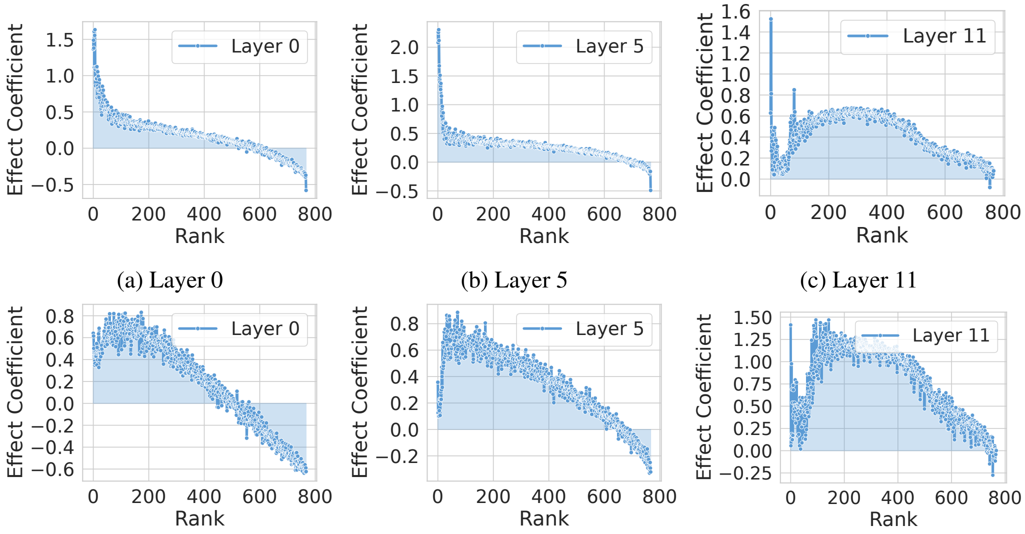

(a) Layer 0
(b) Layer 5
(c) Layer 11
(d) Layer 0
(e) Layer 5
(f) Layer 11

Figure 16: Subspace Cross-Influence that “SVHN” impact on “DTD” at first row and “DTD” impact on “SVHN” at second row.